Summer temperature variability since 1730 CE across the low-to-mid latitudes of western North America from a tree ring blue intensity network

Karen J. Heeter[a,*], Grant L. Harley[a], Justin T. Maxwell[b], Rob J. Wilson[c],
John T. Abatzoglou[d], Shelly A. Rayback[e], Maegen L. Rochner[f], Katherine A.
Kitchens[g]

[a]*University of Idaho, Moscow Idaho, USA.*
[b]*Indiana University, Bloomington, Indiana, USA.*
[c]*University of St. Andrews, Fife, Scotland, UK*
[d]*University of California, Merced, California, USA*
[e]*University of Vermont, Burlington, Vermont, USA*
[f]*University of Louisville, Louisville, Kentucky, USA.*
[g]*University of British Columbia, Vancouver, British Columbia, Canada*

Abstract

Regional reconstructions of air temperature over the past millennium provide critical context for ongoing climate change, but they are temporally limited in the recent period or absent for many parts of the world. We demonstrate the use of latewood blue intensity (LWB) to reconstruct current-year growing (warm) season maximum temperatures (T_{max}) in the low-to-mid latitudes (30°-50°N) of western North America. We present a new tree ring network comprised of 26 LWB chronologies developed from living, high-elevation Engelmann spruce (*Picea engelmannii* Parry ex Engelm.) sampled across the western United States. The LWB parameter shows strong, positive (r =0.65-0.73), and temporally-stable correlations with growing season T_{max}. From this network we present 4 individual T_{max} reconstructions, which characterize regional temperature histories across western North America from northern Mexico to southern British Columbia over the past 4 centuries. Our comparison of these 4 temperature reconstructions highlights the spatial patterns of regional temperature trends throughout time. These reconstructions provide important updates and

---

*Corresponding author

increased data point density to the tree ring temperature proxy network of the Northern Hemisphere. We highlight the use of blue intensity methods at both low- and mid-latitude upper tree line locations to increase the presence of strongly temperature-sensitive records at increasingly lower latitudes of the Northern Hemisphere.

---

1. Introduction

The instrumental temperature record of the past *ca.* 120 years is too short for contextualizing recent temperature trends over longer timescales. Paleoclimate reconstructions, particularly derived from tree ring (TR) records, provide valuable estimates of past temperature variability that extend beyond the observational period (Jones et al., 1998; Mann et al., 1999, 2009; Wahl & Ammann, 2007; Christiansen & Charpentier-Ljungqvist, 2012; Cook et al., 2013; Linderholm et al., 2015; Esper et al., 2018). Currently, the Northern Hemisphere (NH) contains numerous regions that are underrepresented by the coverage of long (*e.g* multi-century) TR-based paleoclimate proxies (Wilson et al., 2016; Anchukaitis et al., 2017; Köse et al., 2017). This study addresses the development of a collection of TR-derived proxy records in a region underrepresented by updated paleo-temperature records—the temperate zone of western North America—and presents a substantial improvement to the spatial coverage of paleo-temperature TR proxy record coverage across the NH paleo-network.

Within the family of paleoclimate proxy records, tree rings are valuable because they provide exactly-dated, well-replicated and sub-annually-resolved data that can extend back in time for multiple millennia, allowing for the analysis of low-frequency variability and trends (Cook & Briffa, 1990; Briffa et al., 2004). As novel dendrochronological techniques are developed and refined, tree rings have become one of the most important sources of late Holocene paleoclimate information, especially in the context of providing information about past hy-

droclimate and temperatures over increasingly longer time periods and across broader areas of the NH (D'Arrigo et al., 2006; Cook et al., 2007; Schneider et al., 2015; Stoffel et al., 2015; Cook et al., 2015; Wilson et al., 2016; Anchukaitis et al., 2017; Esper et al., 2018; Cook et al., 2020). Most large-scale temperature reconstructions are based on either a single index, such as one hemispheric or global mean derived from many points (*e.g.* Frank et al. 2010; Masson-Delmotte et al. 2013) or a spatially-resolved climate field reconstruction, emphasizing regionality before the calculation of large-scale means (*e.g.* Tingley et al. 2012; Anchukaitis et al. 2017).

A synthesis of continental-to hemispheric-scale temperature reconstructions indicates a coherent, unprecedented increase of surface air temperatures within the last century (Mann et al., 1999; Ahmed et al., 2013; Masson-Delmotte et al., 2013). While such large-scale, single-point mean climate indices provide robust, large-scale estimates for attribution studies (Zhai et al., 2018; Stott et al., 2010), they do not perform well for examining regional-scale (100-500 km) temperature variability and relationships with internal modes of climate variability (Neukom et al., 2014; Wilson et al., 2016; Neukom et al., 2019; Christiansen & Ljungqvist, 2017; Maxwell et al., 2020). The challenges associated with the accuracy and reliability of large-scale temperature reconstructions could be due to changes in strength of the predictor-predictand relationship across geographic space (*e.g.* function of distance decay), especially in places where the data network is spatially heterogeneous or sparse. The concurrent assumptions that [1] proxies must be robust estimators of local temperature and [2] the large-scale mean is well-represented by a network of local temperature datasets (Christiansen & Ljungqvist, 2017) may not be well-maintained as the number of records decreases back in time. Relationships between local and NH mean temperatures are largely dependent upon geography, thus, the correspondence of interannual local temperature variability to NH mean temperatures varies across space (Christiansen & Ljungqvist, 2017). To account for regional variability that is often muted in large-scale reconstructions, finer-scale models offer the benefits of more accurately characterizing local-to-regional scale climate variability and

4

geographic expressions of atmospheric circulation patterns, radiative forcing, and ocean-atmosphere variability (Anchukaitis et al., 2017).

Across the NH, TR-derived temperature reconstructions are most highly concentrated at high latitudes (>50°N), where temperature is expected to be the most limiting factor on tree growth (*e.g.* Fritts 1976; Jacoby & D'Arrigo 1989; Briffa et al. 1992, 2001; Anchukaitis et al. 2013; Wilson et al. 2014; Björklund et al. 2014; Rydval et al. 2014; Linderholm et al. 2015; Björklund et al. 2015; Wilson et al. 2017; Rydval et al. 2017; Fuentes et al. 2018; Wilson et al. 2019; Björklund et al. 2019). At high latitudes, spatially-resolved TR proxies have been applied successfully for the evaluation of past temperature forcing by volcanism (Anchukaitis et al., 2017; Edwards et al., 2021) and the timing and amplitude of past cool and warm events such as the Medieval Climate Anomaly (MCA), the Little Ice Agre (LIA), and the 20th-21st century warming trend (D'Arrigo et al., 2006; Schneider et al., 2015; Wilson et al., 2016). The same principle of temperature as a limiting factor for trees at high-latitudes (*e.g.* D'Arrigo et al. 2001; Gervais & MacDonald 2001; Porter et al. 2013), also applies in high-elevation zones of low-to-mid-latitude, montane environments.

Recent progress to broaden the latitudinal extent of the NH TR temperature proxy network to the lower latitudes (< 45°N, *e.g.* Briffa et al. 2001; Büntgen et al. 2008; Dorado Liñán et al. 2012; Büntgen et al. 2017; Heeter et al. 2019; Esper et al. 2020; Reid & Wilson 2020; Heeter et al. 2020; Harley et al. 2020a; Büntgen et al. 2005; Fan et al. 2009; Buckley et al. 2018) can be attributed to [1] an increased number of investigations of high-elevation, temperature-sensitive trees, and [2] the development and application of additional TR metrics other than tree ring width (TRW) such as maximum latewood density (MXD; Schweingruber et al. 1978) and blue intensity (BI; McCarroll et al. 2002). These studies demonstrate that when TRW serves as a weak temperature predictor due to complex climate-growth relationships at lower latitudes (<40°N) (George & Ault, 2014; Fritts, 1976; Wilson et al., 2016; Büntgen et al., 2008; Reid & Wilson, 2020), ring-density parameters (*e.g.* MXD and BI) can still be strongly representative of local to regional temperatures.

Over the last decade, BI-derived temperature proxies have become important additions to the MXD and TRW temperature proxy network across the NH. BI uses the light absorbance properties of wood compounds that comprise the cell walls (*e.g.* lignin) to obtain a measure of raw light reflectance across the earlywood and latewood zones of an annual growth ring. Examination of minimum BI by McCarroll et al. (2002) showed the latewood reflectance exhibited a strong, negative relationship with MXD (r = -0.95, p <0.01), and thereby were the first to suggest that BI could be an important and effective surrogate for MXD to examine annual to decadal-scale changes in temperature. As raw BI measurement data are inversely correlated with MXD (*i.e.* a dense, dark latewood will express low reflectance), current protocol inverts the raw latewood BI (latewood blue intensity; LWB) to allow the same detrending procedures to be used for both LWB and MXD data (Wilson et al., 2014; Rydval et al., 2014). As such, the LWB metric response to summer maximum temperature (T_{max}) is typically very similar to that of MXD. Aside from exhibiting stronger, positive relationships with instrumental summer temperature data than TRW (*e.g.* Wilson et al. 2014), both MXD and LWB are shown to exhibit less signal contamination from biological memory of non-climatic factors and express similar auto-correlative properties to the instrumental data (Esper et al., 2014; Rydval et al., 2018; Lücke et al., 2019).

Continued efforts by the paleoclimate community to develop and archive robust temperature-proxy data are apparent by chronology network syntheses (*e.g.* Briffa et al. 1988, 1992; Schweingruber et al. 1993; Schweingruber & Briffa 1996), and most recently, the creation of NTREND-2016, a publicly available multi-TR-proxy dataset (Figure 1), as well as the PAGES 2K multi-proxy dataset (Consortium et al., 2017). While the spatial representation of paleo-temperature proxies in many parts of the low- and mid-latitudes of the NH continues to improve, many of these pre-existing proxies do not include the most recent period (*e.g.* Briffa et al., 2001); currently only a few TR based temperature reconstructions from the low-to-mid-latitudes of the NH extend past *ca.* 1990. As such, many of these records cannot be calibrated with in-

strumental climate data over the last *ca.* 20–30 years—a period characterized by unprecedented and extreme climatic trend. Therefore, temperature-sensitive records that extend to the most recent period are valuable, because they provide a more complete understanding of climate-tree growth relationships and past climate variability (Larson et al., 2013).

To date, few TR-based temperature reconstructions, which characterize historical regional temperature variability, exist for the western continental United States (US) (Douglas & Stockton, 1975; Graumlich & Brubaker, 1986; Briffa et al., 1992; Graumlich, 1993; Biondi et al., 1999; Salzer et al., 2014a; Heeter et al., 2020, 2021; Martin et al., 2020). However, most of these records end prior to *ca.* 2000, and thus do not contextualize recent warming trends. The western US is a region within the NH where improvements to the temperature proxy network are needed both spatially and temporally. In this paper, we present a temperature-sensitive TR proxy network comprised of LWB records from 26 sites across the western US. We use this new network to produce 4 regional reconstructions of growing-season T_{max} that represent the spatial temperature variability not only across the low-to-mid latitudes of the western US, but also throughout southern Canada and northern Mexico. Temporally, these regional reconstructions include the most recent decade (post 2010 CE) and span several hundred years back in time. The temporal span of these reconstructions is valuable in that they track recent trends in regional temperature and their multi-century contextualization. Further, we emphasize the potential for BI parameters to fill data gaps in other low-to-mid-latitude regions globally.

2. Methods

2.1. Study location

Data for this study are derived from a network of 26 sample sites across various regions of the western continental US (Figure 1; Table 1). All site-level TR chronologies are derived from living Engelmann spruce (*Picea engelmanni* Parry ex Engelm.). Sites were visited between 2001 and 2020, with the major-

ity of samples collected during the summers of 2017 and 2018. At each site, we used a hand-held increment borer to extract cores from 10 to 25 living trees, with 2 cores taken per tree at 1.3 m above the ground. We targeted *P. engelmannii* for this study, because this species is widely distributed across the most temperature-limited environments (elevations >3,000 m) of the western US. Further, *P. engelmannii* was shown previously to be favorable for BI methods due to its light-colored wood, characterized by a lack of a visual color change between heartwood and sapwood, and a lack of resin content (*e.g.* Wilson et al. 2014; Heeter et al. 2020).

2.2. Sample preparation and data collection

Each core sample was processed with the intent of collecting both TRW and LWB data. As such, we followed careful BI sample protocols to ensure high quality surface preparation, including achieving a flat sample surface plane and the removal of samples exhibiting discoloration due to resin content or fungal staining. After collection, cores were dried and mounted in the lab. Given that BI measurements can be affected by the presence of mobile wood compounds not confined to an individual annual ring, such as water and resins, chemical-based resin extraction is often required prior to BI measurement (*e.g.* 24 °C 99.5% acetone bath; Rydval et al. 2014; Buckley et al. 2018). Because the radial sections of *P. engelmannii* cores were typically free of excessive resins and were uniformly light-colored with no obvious heartwood/sapwood color change, the samples for this study were not chemically treated. However, in recent decades, widespread activity from high-density populations of spruce beetle (*Dendroctous rufipennis* Kirby [Coleoptera: Scolytinae]) has caused large-scale forest disturbances across western North America. The fungal symbiont most frequently associated with spruce beetle (95% of individuals) is *Leptographium abietinum* (Peck) M.J. Wingf. (Aukema et al., 2005; Cardoza et al., 2008; Six & Bentz, 2003), a blue-staining endophloedic species (Davis et al., 2018). *P. engelmannii* are particularly prone to discoloration from blue-stain fungus, which presents a potential problem for measuring BI on this species. For this reason, we avoided

sampling any trees with evidence of spruce beetle infestation. Cores were also examined for any evidence of blue staining and omitted from further analysis if present.

After examining cores for discoloration, we saturated the cells of the mounted samples by brushing the surfaces with water. We incrementally shaved all saturated samples with a core-microtome until a flat planar surface was achieved (Gärtner & Nievergelt, 2010). Lastly, all shaved samples were polished with 40 micron sanding paper and treated with compressed air to remove any residual sawdust particles from the intercelluar pores or cracks in the wood.

Prepared samples were scanned as JPEG images on a calibrated Epson 12000 XL flatbed scanner at 3200 dpi. We initially calibrated our scanner using the Silverfast software in combination with an IT8 7.2 calibration card. We then measured TRW of the scanned cores to 0.001 mm precision using the software CooRecorder (Larsson, 2014). After all samples were measured, visual TRW cross-dating was statistically validated using the software COFECHA (Holmes, 1983). After absolute dating was established with TRW, we obtained LWB data for all samples in CooRecorder (Cybis, 2020).

2.3. Chronology development and regionalization

We developed TRW and LWB chronologies for each of the 26 sample sites, totalling 52 chronologies. As all chronologies showed non-climatic, growth-related age trends (Fritts, 1976), we compared multiple approaches to series detrending (*e.g.* Negative Exponential, Age-dependent, 2/3 spline) in both the ARSTAN (Cook & Holmes, 1996) and SignalFree (Melvin & Briffa, 2008) frameworks. The examination of multiple detrending options revealed minimal differences between chronology variants, however, we found that the best chronologies were consistently produced when calculated as power-transformed residuals (rather than ratios) in the SignalFree (SF) framework, detrended with the Age-dependent spline (SF-ad); we applied SF-ad detrending to all chronologies in the network. We used an expressed population signal (EPS) value of 0.85 to identify the period when chronology sample depth is not representative

of the theoretical perfect chronology. Common signal fidelity of each chronology was assessed using the RBAR (average correlation between series; Fritts 1976) value.

We examined the spatio-temporal relationships between the detrended TRW and LWB chronologies and local (within 0.5°of the sample location) CRU TS 4.04 0.5°(land) T_{mean} and T_{max} data (Harris et al., 2014) using a Pearson correlation analysis in KNMI Climate Explorer (Trouet & Van Oldenborgh, 2013) over the period spanning 1920−present. This period best reflects when the representation of high-elevation areas by montane, climate-data stations is most-reliable and consistent across the western US. Because the TRW chronologies showed consistently weak correlations with CRU T_{mean} and T_{max} (Harris et al., 2014) (see section 3.1; Figure S1), we focus the remaining description of methods to LWB predictors.

We sorted all LWB chronologies into sub-regional groupings using a 2 step process. First, we assessed the spatial homogeneity between all chronologies using principal component analysis (PCA; Husson et al., 2016) over the common period shared by all 26 chronologies (1920−2000). Following the Kaiser-Guttman rule (Guttman, 1954; Kaiser, 1960), we retained the first n eigenvectors with eigenvalues >1.0. The network-wide PCA on the 26 LWB chronologies resulted in 3 PCs with eigenvalues >1.0, explaining a cumulative 68.5% (PC1: 45.2%, PC2: 14.4%, PC3: 8.9%) of the overall variance amongst the LWB chronologies. Second, regional groupings were defined using a complete linkages hierarchical cluster analysis (HCA) (Revelle, 1979) on a Euclidean distance matrix created from loading values of LWB chronologies to the final subset of PCs using the R package FactorMineR (Husson et al., 2016). Results of the complete linkage HCA on the loading values of the chronologies to $PC_{1−3}$ suggested optimal level of division was achieved at a height of 0.70 (Figure S2). This division level allowed us to group chronologies into 4 geographic regions: the Northern (NR), Central (CR), and Southern Rocky Mountains (SR), and the Intermontane Plateau (IP).

Once individual chronologies were sorted into regions, we examined each site

chronology against regionally-averaged CRU TS 4.04 0.5°temperature (T_{max}, T_{mean}), precipitation, and self-calibrating Palmer's Severity Drought Index (scPDSI) spatial data fields (Harris et al., 2014) for each region in Climate Explorer. Since LWB predictors consistently showed the strongest relationships with regionally-averaged CRU T_{max} over the common instrumental period (Figure 2; Figure S3), we proceeded with the CRU T_{max} dataset for the subsequent reconstructions. To determine the target seasonality of the subsequent reconstructions, we compared Pearson correlations across multiple months to determine which combination of months would result in the strongest positive relationship between the instrumental record and the predictors for each region.

2.4. Regional reconstruction models

Using the regional groupings identified by the HCA, we developed 4 regional T_{max} reconstructions using a nested principal components regression (PCR) approach, which accounts for the decrease in number of predictor chronologies back through time (Cook et al., 1999). Across each regional grouping, we initially pre-whitened the predictor LWB chronologies and CRU T_{max} data to provide a conservative estimate of climate-predictor relationships that are not subject to inflation via auto-correlation. Chronologies were retained for modeling if they were positively and significantly ($p<0.05$) correlated to the regionally-averaged target temperature data during the common period (shared by the CRU T_{max} data and the chronology) using the Pearson, Robust Pearson, and Spearman correlation coefficents (Table S3). The original chronologies (non-pre-whitened) of significant predictors were then used in the PCR to develop the reconstructions. Following the Kaiser-Guttman rule, the first n eigenvectors with eigenvalues >1 were retained for the PCR. We determined the final subset of PCs by using the minimum Akaike information criterion (AIC), which includes a penalty term for increasing the number of predictors in the model (Akaike, 1974).

We use 1920 as the starting year of the common calibration period because prior to this date, there are many places across the western US where representation of high-elevation areas by montane, climate-data stations is scarce or

inconsistent. For this same reason, a similar starting year for the calibration period was used for the temperature reconstruction by Heeter et al. (2020) in north-central New Mexico, US. The end of the common calibration date depends on the common period shared by all predictors of each region. The seasonality of each regional reconstruction was determined by performing a series of regression experiments between target CRU temperature data and the LWB predictors. For each region, we split the instrumental period into 2 periods ("early" and "late") to validate and cross-validate the reconstruction model, as well as to test for stability over time (Table 2). We performed model validation by calculating cross-calibration statistics for the full period and verification statistics for the early period. This practice is common, as the earlier portions of the instrumental record often possess greater uncertainty than the latter part of the record (Cook et al., 2013) We used 2 goodness-of-fit tests to validate the models: the reduction of error (RE) and coefficient of efficiency (CE) (Fritts, 1976; Cook et al., 1999). When RE values (ranges from $-\infty$ to +1) are positive, the calibration model is a more skillful predictor of the target data than the mean of the instrumental data during the calibration period. Although CE has the same range and calculation, a positive CE value is more difficult to obtain because it relies on the verification period mean for a baseline of predictive skill. The validation statistics produced were the calibration and verification period coefficient of determination (CRSQ and VRSQ), and the validation period reduction of error and coefficient of efficiency (VRE and VCE). To quantify model uncertainty, we used the maximum entropy bootstrapping method (MEBoot) (Vinod et al., 2009) to produce 300 reconstruction replicates.

2.5. Reconstruction analyses

We first transformed reconstructed values to anomalies calculated over the full period of each reconstruction. We then calculated the top 5 single-year cool and warm anomalies for each regional reconstruction. We conducted a severity-duration analysis (González & Valdés, 2003) on reconstructed values of at least 2+ years to determine the magnitude (average cumulative departure

from the long-term mean), duration (time span of each event), and intensity (duration divided by the magnitude) of warm and cool events. Duration and magnitude of each event were ranked and compiled to give each event an overall rank score. The top 5 warm and cool events are based on the overall score. We quantified and assessed the degree of between-group and within-group synchrony (the estimated proportion of common inter-annual variance; $\hat{a}_c$) of each regional reconstruction using the Dendrosync package in R (Alday et al., 2018). In order to better visualize and compare decadal trends across each region, we also transformed reconstructed values for each time series into z-scores based on the mean and standard deviation of the common reconstructed period and applied an 11-year running average smoother. We additionally compared correspondence between our record and other regional and hemispheric-scale temperature reconstructions using a Pearson's correlation analysis over the common period of all reconstructions.

3. Results and Discussion

3.1. LWB as a temperature proxy in western North America

The preliminary response of the individual LWB chronologies and their TRW counterparts to local temperature data consistently shows that LWB chronologies exhibit a stronger relationship with current-year growing (warm) season temperatures than TRW (Figure S1). With the exception of a few sites, the LWB chronologies in this network are not highly correlated with their respective TRW site chronologies (Table S1). While Salzer et al. (2014a) demonstrate that TRW can be a successful parameter for developing a low-frequency temperature reconstruction for a nearby region of North America (Great Basin), our findings highlight the utility of BI methods for creating temperature-sensitive proxies from tree rings when conventional TRW series do not show as strong of correlations with instrumental temperature data. We initially experimented with using both TRW and LWB for the proposes of reconstructing temperature, but the addition of the few TRW chronologies that were significantly ($p<0.05$),

13

but weakly correlated to temperature, to the predictor pools did not lead to any improvements in the models achieved when solely using LWB predictors. Briffa et al. (1992) reported similar findings while experimenting with the inclusion of TRW predictors in their MXD-based temperature network for the western US. Like the presentation of the MXD network presented by Briffa et al. (1992), proceeding with just the LWB predictors allows us to better emphasize the efficacy of the LWB metric for the creation of this temperature-sensitive TR network.

The replication needed to attain the 0.85 EPS threshold ranges from 3−13 trees, with an average of 6 trees. RBAR values range from 0.26−0.65, with an average of 0.36 (Table 1). These chronology statistics are consistent with findings from Wilson et al. (2014), who presented BI-derived temperature reconstructions using *P. engelmannii* from 7 sites across southern British Columbia, Canada.

At the local scale (within 0.5°of each site), the LWB chronologies exhibit higher correlations with T_{max} than with T_{mean}, which is consistent with other BI and MXD studies in North America (*e.g.* Wilson & Luckman 2003; Luckman & Wilson 2005; Wilson et al. 2014, 2019; Heeter et al. 2020; Harley et al. 2021). All temperature-LWB relationships are time-stable (Table 1). While sampling protocol aimed to avoid specimens visibly or knowingly influenced by ecological disturbance, we suspect that the chronologies at 3 sites (ABA, PLS, TUS) show the effects of heightened spruce beetle (*Dendroctonus rufipennis* Kirby) outbreaks in southern Utah during the turn of the 21st century (DeRose et al., 2011). The original sample collections from these 3 sites contained multiple cores which were omitted due to the presence of blue staining across the outermost growth rings. For this reason, we truncated ABA to 2002, PLS to 2000, and TUS to 2011. Because linkages have been shown between increased temperatures, heightened spruce beetle outbreak severity, and *P. engelmannii* mortality (DeRose et al., 2013; Pettit et al., 2020), targeting this tree species for future temperature reconstructions across the western US may warrant additional consideration of site-level land use and examination of disturbance histories (Trotsiuk et al., 2018).

3.1.1. Regional-level climate response

All LWB chronologies show significant ($p<0.05$) and positive responses to CRU T_{max} during at least 2 current-year growing season months (Figure 2). Across most regions, statistically significant ($p<0.05$) temperature response begins in March or April, and the optimum seasonal window concludes with September. For all regions, the strongest relationship between T_{max} and the LWB chronologies over a single month occurs in August. This was expected, as the relationship between LWB and temperature has been widely shown to be strongest in late-summer months (Wilson et al., 2014; Heeter et al., 2020; Rydval et al., 2017; Wilson et al., 2019; Wiles et al., 2019; Heeter et al., 2021).

Notably, the IP chronologies exhibit optimum response in the months of April, May, and August, with the June and July response being weak. Compared to the other 3 regions, the IP region simultaneously experiences the least amount of monthly precipitation and the highest mean and maximum temperatures during the mid-summer months (June and July) (Figure S4). We suspect that the decreased temperature response of IP LWB chronologies in June and July may be resultant of mid-summer temperatures exceeding the tolerance limits of trees in this region. The IP chronologies, many of which are located in the arid regions of southern Utah, exhibit the most strongly-negative correlations with regional target CRU scPDSI than any other region during June and July (Figure S3). Despite this characteristic, the IP chronologies do not show significantly negative correlations with precipitation during these months. Therefore, we suspect that the decreasing temperature response trend is less likely an artefact of a competing hydroclimate signal. A similar pattern of decreased mid-summer temperature response is also apparent with the NR LWB chronologies. However, unlike in the IP, where low precipitation is likely a limiting factor year-round regardless of temperature, the NR receives significantly less precipitation in June and July. The NR LWB chronologies show significant negative correlations with precipitation during these 2 months, thereby suggesting that this trend may be influenced by a competing hydroclimate signal during the mid-summer months.

Similar effects of reduced TR temperature-sensitivity during mid-summer can be seen in the LWB predictors developed in southern British Columbia and Alberta by Luckman & Wilson (2005) and Wilson et al. (2014). Büntgen et al. (2017), who use MXD to reconstruct summer temperatures in the Spanish Pyrenees, suggest that a weakening of TR temperature sensitivity in mid-summer months due to increased drought stress likely occurred whenever past summers were exceptionally warm and dry.

The SR chronologies express a strong temperature response, but over the shortest season compared to the other regions. This response may be impacted by the hydroclimate and evaporative demands related to temperature on TR growth in this region, as well as is likely artefact of negative correlations between T_{max} and precipitation in this region during non-monsoonal months. Babst et al. (2016) suggest that annual growth of high-elevation conifers in the southwest US are primarily reliant on spring and monsoon precipitation, rather than winter precipitation. We suspect that the strong monsoonal influence of the SR during July−September (Figure S4; US Climate Data 2020) is potentially influencing the onset and duration of seasonal temperature response in this region. Additionally, the *P. engelmannii* collected from some of the sites in the SR region (*e.g.* LOS) exist as disjunct populations near the southernmost extent of the species geographic range (Little & Viereck, 1971). The shortened duration of strong temperature response of southernmost chronologies within the SR supports the principle of ecological amplitude (Griggs, 1914; Fritts, 1976; Holt & Keitt, 2005). This spatial pattern suggests that there may be differences in tree sensitivity to temperature between individuals toward the southern range periphery versus those toward the center of the species range and, further, may be evidence of the role of temperature in how climate change influences future species distribution patterns (Thuiller, 2004; Hill et al., 2011).

We found that the optimum target season for the NR is May-August (MJJA), the CR is May-September (MJJAS), the IP is April-September (AMJJAS), and the SR is August-September (AS) (Figure 2; Table S2). Notably, the IP shows highest *r*−values ($p<0.05$) when April and May are included. Most of the

regional chronology pools display the highest r-values when computed over a longer growing season comprised of multiple months. The SR is the exception, displaying highest r-values when computed over 2 consecutive months in the late growing season (August and September). This finding is consistent with prior results indicating reduced temperature response of LWB to earlier growing season temperatures in this southernmost region (Heeter et al., 2020).

The differences in seasonal duration of the *P. engelmannii* LWB response to T_{max} across the historical species range (Figure 1; Little & Viereck 1971) is likely attributable to factors such as [1] distance to upper tree-line (Lloyd & Fastie, 2002; Salzer et al., 2014b; Elliott, 2011; Kipfmueller & Salzer, 2010), [2] proximity to the interior versus the periphery of the range (Amburgey et al., 2018; McCullough et al., 2017; Herrero et al., 2013), or [3] differences in the timing of cambial reactivation (indicating start of the growing season) (Deslauriers et al., 2003; Begum et al., 2010; Gruber et al., 2009; Harley et al., 2012) based on location. Regardless of cause, differences in seasonal response can be problematic for equitably comparing temperature responses of chronologies comprising broadly-distributed temperature proxy networks. Similarly, differences in seasonality of temperature response at the local level has important implication for studies emphasizing spatial analysis of climate proxies (*e.g.* Anchukaitis et al. 2017), which use a common seasonal target over a broader area; in the case where the optimum seasonal target for reconstruction differs across space, calibration results of the spatially-resolved version of the reconstructions may appear weaker than calibration results of more localized reconstructions with variable seasonal targets, such as this study. As such, differences in seasonal response should also be taken into account when comparing TR temperature predictors across regions.

3.2. Reconstruction models

3.2.1. Model validation

Calibration and verification statistics are summarized in Table 2. The last year of the common calibration period of each model ranges from 2000–2015.

The IP common calibration period ends in 2000, because several chronologies in this group are truncated due to issues of ecological disturbance in the most recent years of growth. The NR common calibration period is simply limited to the earlier sample date of one of the NR chronologies (FKY). Although FKY does not extend past the year 2000, the scarcity of temperature-sensitive records in this part of North America warrants its inclusion. Forward nests were then applied as needed: 1 for the NR, 3 for the CR, 4 for the IP and, and 2 for the SR (Table 2; Table S4). The nested PCR models retain only the first PC for the NR, CR, and IP models, with PC1 explaining 71.2%, 79.5%, and 68.1% of the respective cumulative variance for each model. The PCR process retains the first 2 PCs for the SR, with PC1 (59.7%) and PC2 (13.4%) explaining 73.1% of the cumulative model variance. These results reflect the strong common temperature signal among intra-regional predictors identified by the HCA.

3.2.2. Model strength and timespan

The timespan of each model varies, with start year of each reconstruction occurring between the period 1623−1730 (Table 2). VRE and VCE statistics are positive for all nests across the entire reconstructed period (Table 2; Table S4) for each region, indicating that all reconstructions are skillful estimates of temperature through time (Cook et al., 2013). All reconstructions cover the most recent decades, spanning to 2018. To date, there are few published tem-perature reconstructions that adequately capture the first 2 decades of the 21st century in the calibration period (*e.g.* Fuentes et al. 2018; Heeter et al. 2020; Keyimu et al. 2020a,b; Heeter et al. 2021). RSQ values indicate robust model strength for each region, explaining at least 44% of the common period temper-ature variance (Table 2; Table S4). Model strength for these 4 reconstructions are comparable to other BI- and MXD-based temperature reconstructions for North America (Briffa et al., 1992; Wilson et al., 2014, 2019; Heeter et al., 2020). Comparatively, the SR model shows the strongest overall skill, explaining 54% of the overall instrumental temperature variance of the most well-replicated nest (1878-2014). While the CR is comparatively the weakest and shortest model,

it still accounts for 44% of the temperature variance of the most well-replicated nest (1850-2015).

The relationships between the LWB chronology predictors and CRU T_{max} data also show strong spatial correlations (Figure 3). We noted only slight increases in spatial correlations between non-transformed data and the first-differenced data, indicating that the LWB response is strong at both the inter-annual and multi-decadal timescales. While the highest correlations are centered over the immediate study areas, thereby highlighting the sub-regional differences in T_{max} patterns across the western US, these data are strongly representative of ($r > 0.60$, $p<0.05$) maximum temperature across the entire western US, north-west Mexico, and parts of southern Canada. The broad spatial implications of these results suggest the possibility to extend the NH TR based temperature proxy network southward, as previously highlighted by Heeter et al. (2020). Similar efforts to increase coverage of under-represented areas will allow for a better understanding of the spatial patterns of historical temperature variability across broader geographical space.

3.3. Reconstruction analysis

3.3.1. Analysis of historical temperature variability

The 4 reconstructions show similar evidence of warm and cool periods but differ with regards to the onset, duration, and intensity of these periods (Figure 4; Figure S5). We suspect that the differences among regions with regards to the magnitude and duration of warm and cool events can somewhat be attributed to the varying seasonal targets of each reconstruction. The instrumental record indicates strong spatial coherence of surface air temperatures across the western US within the last century, which is well-reflected by the 4 reconstructions. Notably, all regional reconstructions capture a substantial warming trend beginning at the end of the 20th century into the present. The recent warming period of *ca.* 2000 to present, documented by the instrumental record, has somewhat limited representation by NH temperature proxy studies due to insufficient record length (*e.g.* Wilson et al. 2016; Anchukaitis et al. 2017).

Specifically in western North America, the most recent decades are characterized by not only an unprecedented increase in surface air temperatures, but also anomalous drought, streamflow declines, increased wildfire activity, and reduced annual snowpack (Cook et al., 2004, 2008; Kalra et al., 2008; Pederson et al., 2011; Abatzoglou & Williams, 2016; Harley & Maxwell, 2018; Williams et al., 2020; Harley et al., 2020b). The severity-duration analysis indicates that, despite the short duration, high magnitude rankings places 2015−2018 within the top 10 overall ranking warm events, and as the most intense event for the CR, IP, and SR regions (Table 3). The year 2017 is ranked among the 10 warmest single-year anomalies over each reconstructed period for all regions, and in the top 5 for the CR, IP, and SR. While the CR, IP, and SR reconstructions slightly overestimate the warming of 2017, the relative ranking of warm years spanning the period 2015−2018 is well corroborated by the instrumental record (Figure 3). Our ability to capture the period post *ca.* 2010 in the TR temperature proxy record for model calibration is meaningful, because it allows us to more accurately place the most recent period, characterized by severe trend, into historical context. Further, the strong correspondence between the instrumental and LWB data during the modern warming period (Figure 3) instills additional confidence in extending the tree ring records back in time to robustly provide estimates of other anomalously warm periods such as the MCA. Considering the serious implications of the projected continual warming (Flato et al., 2013), precise, updated proxy records are important for improved detection and attribution studies related to temperature trends and for constraining models of future temperature change.

Another pattern captured across the majority of the regions is the cooling experienced between *ca.* 1960−1980. This period has widely been related to a time of global solar dimming (Wild, 2009). This cooling event in the 20th century is most intensely and continuously experienced in the CR and SR regions and may have implications for solar forcing attribution studies in North America. During this time, the IP oscillates between moderately cool (z-score >-1.0) and slightly warm (z-score <0.50) periods, while the NR shows the predominance of

slightly cool (z-score >-0.5) years. The period of *ca.* 1965−1980 is represented in both the 5 coldest single-year anomalies or the top 5 overall ranking cool events for each region. Notably, 1965 is both the single coldest year anomaly captured by both the instrumental data and reconstruction for the IP.

Another major warm period that is well documented across all regional reconstructions occurred in the 1930s. This anomalous warming is often associated with the Dust Bowl, a period of extreme drought across the western US (Cook et al., 2008; Woodhouse et al., 2010). Conditions during certain years of the Dust Bowl rival the modern warming, as the period spanning *ca.* 1928−1942 appears within the 5 top-ranking warm events for the NR, CR, and IP reconstructions. The magnitude of the Dust Bowl is comparatively strongest in the CR region, with z-scores > 1.0 for this period. The period 1928−1940 is the top-ranking warm event for the CR reconstruction. The CR differs from the other 3 regions in that the Dust Bowl warming appears to have been an abrupt change from moderately cooler years in the early 20th century to very warm years, as opposed to a continual warming trend since *ca.* 1900 that culminated in the 1930s and 1940s (Figure 4). The Dust Bowl is less pronounced in the SR, as *ca.* 1928−1940 is situated towards the terminus of a nearly continuous warm period since *ca.* 1830.

The 4 regions show cooling around the time of the Dalton Minimum (*ca.* 1790−1830; Wagner & Zorita 2005; Bond et al. 2001), which is widely described by numerous other temperature proxy studies of the NH (*e.g.* Briffa et al. 1998; Büntgen et al. 2005). While the cooling during the Dalton Minimum was historically attributed to solar forcing, in many areas, this period is primarily attributed to volcanic forcing (*e.g.* unknown 1809 event, Mt. Tambora eruption of 1815; Wagner & Zorita 2005; Hegerl et al. 2011; Gennaretti et al. 2014; Schurer et al. 2019). The cooling effects of volcanic eruptions during this time are widely documented in the TR record across North America (D'Arrigo & Jacoby, 1999; D'Arrigo et al., 2013; Stoffel et al., 2015; Wilson et al., 2016). Cooling begins approximately just after *ca.* 1790 for the majority of regions and lasts into the 1840s. All regions show 2 distinct pulses during this period, the former spanning

ca. 1790−1820, and the latter spanning *ca.* 1825−1845. The second pulse is most intensely expressed in CR, with the period spanning 1834−1849 ranking as the top coldest event for the region.

The Maunder Minimum (*ca.* 1645−1715; Eddy 1976), another cooling period attributed to solar forcing and volcanic activity (Lean et al., 1992; Shindell et al., 2001; Crowley et al., 2008), is less pronounced than the Dalton Minimum in IP and SR. The length of NR and CR precludes examination of this time period. IP characterizes the Maunder Minimum as oscillating between moderately warm and cool periods instead of a continuous cooling, whereas SR documents continuously warm temperatures interrupted by an intense cooling spanning the period *ca.* 1635−1655. IP indicated 2 of the 5 top-ranking cool events spanning the periods 1654−1659 and 1676−1678 occur during the Maunder Minimum. Similarly, the period spanning 1641−1656 is the top-ranking cool event for SR. While the Maunder Minimum can be seen in numerous longer-term reconstructions of temperatures of the extra-tropical NH, (*e.g.* Briffa et al., 2001; Esper et al., 2002; Wilson et al., 2016) the presence and magnitude of these past events are not ubiquitous across different regions and scales (Anchukaitis et al., 2017). Spatial differences can be seen at the sub-continental level as well; within North America, paleo-temperature records from the Gulf of Alaska and the Alberta Icefields show the period *ca.* 1690−1710 CE as being anomalously cold and attributed to volcanic activity (Luckman & Wilson, 2005; Wiles et al., 2014), while this period is only somewhat evident in the IP record and absent in the SR record. Like with the Dalton Minimum, non-ubiquitous observations of the Maunder Minimum are likely resultant from heterogeneous climatic effects of volcanism over space. Studies suggest that temperature forcing of many of the largest, high-latitude volcanic eruptions of the past *ca.* 1200 years (*e.g.* 1783 Laki), are varied globally (Zambri et al., 2019; Schmidt et al., 2012; Oman et al., 2006). Specific to western North America, while Crowley et al. (2008) did not find a global expression of the Laki eruption, Jacoby et al. (1999) and Edwards et al. (2021) both show cooling effects from Laki across northern Alaska. Further, Shindell et al. (2001) attribute non-ubiquitous observations of the Maunder

Minimum, particularly over North America, to lowering indices of the Arctic Oscillation/North Atlantic Oscillation as solar irradiance decreases in this period.

The majority of examinations into the effects of volcanism on surface air temperatures in the NH are, to date, largely dependent on MXD chronologies. We suggest that LWB may be an additional suitable parameter for future quantification of volcanic cooling at finer timescales (*e.g.* seasonal or sub-seasonal), because like MXD, the temperature response of LWB is less likely to be influenced by biological persistence than with TRW (D'Arrigo et al., 2013; Stoffel et al., 2015; Lücke et al., 2019; Reid & Wilson, 2020). Recently, Edwards et al. (2021) use a combination of quantitative wood anatomy (QWA; von Arx et al. 2016) and climate modelling to show that the effects from the 1783 Laki (Iceland) eruption across northern Alaska were more accurately characterized as an abrupt decrease in temperature at the end of the growing season, as opposed to an entire growing season that was anomalously cool. As such, the application of novel TR parameters such as BI and QWA will likely play an important role in future examination of the effects of volcanic cooling across different spatial and temporal scales. As suggested by D'Arrigo et al. (2013), the quality, type, and spatial distribution of chronologies averaged together to derive larger-scale estimates of past temperature are important to ensure that any volcanic signal is not muted. Attempts to decrease uncertainty in larger-scale estimates of temperature by increasing spatial coverage of temperature-sensitive TR chronologies will be welcome, particularly in the estimation of volcanic cooling.

3.3.2. Reconstruction synchrony and large-scale comparisons

While all 4 records show similar decadal trends, an examination of changes in the synchrony of trends are important to better understand how internal modes of variability result in changes to local climate over geographic space and time. Unlike correlation analysis, which provides a measure of similarity between the calculated means of individual timeseries over a given period (*e.g* 10 year period), the additional value of analyzing timeseries synchrony is that it allows for examining the relative timing of climatic events and the likelihood that

such events will occur at the same time (*e.g.* extreme hot or cold years). Over the common period of all 4 regional models (1730−2018), trends in between-group synchrony of temperature anomalies show patterns of spatial-dependence. For example, the IP and SR show the highest between-group synchrony, and the NR and SR show the least (Figure 5A). Notable periods of increasing synchrony across all 4 records include the latter half of the 20th century, specifically the Dust Bowl, and the period between the Dalton Minimum and the terminus of the LIA (Figure 5B,C). The strongest decline in overall synchrony between the 4 regions occurs around the turn of the 20th century following the LIA (*ca.* 1880−1920). Although the Rocky Mountain models (NR, CR, and SR) show strong coherence during this time, the overall declining trend is driven by strong decreases in synchrony between IP and the Rocky Mountain models. This trend reflects the complexity of land surface temperature changes across geographic space during a climatic transition period characterized by substantial changes to relative external forcing by atmospheric and oceanic circulation patterns (*e.g.* AMO, PDO), as well as increased anthropogenic influence at the end of the LIA (Kreutz et al., 1997; Knudsen et al., 2014; Brönnimann et al., 2019). Future studies examining historical periods of asynchronous temperature trends across western North America are needed to more fully understand the effects of broad-scale ocean/atmospheric forcings on internal modes of temperature variability for this region.

The ability to compare our records with other regional and hemispheric-scale reconstructions provides evidence to better understand the relationship between volcanism, atmospheric circulation, and changes to surface air temperatures across space, especially at lower latitudes. Our records show strong agreement with nearby temperature records from North America (Figures 6A, 6C). The strongest agreement between the 4 records we present and the MXD-based temperature record for the western US by Briffa et al. (1992) is not surprising given the similarities between LWB and MXD, as well as the close spatial proximity of the records. Similarly, the coherence of the NR record with the British Columbia and Alberta records by Wilson et al. (2014) and Luckman & Wilson

(2005) is expected given the location and similar type and seasonality of these records. As such, we emphasize the importance of independent validation of previous studies within the region. Since many of these pre-existing temperature proxy records for North America do not extend to include the most recent decades, our corroborating records provide valuable updates to this region of the NH temperature proxy network.

To date, many ensemble reconstructions, providing estimates of historical temperature variability, exist for the NH. However, there is poor representation of temperature-sensitive predictors from the mid-latitudes of North America in these ensemble reconstructions. We compare decadal trends for each of the regional reconstructions presented in this study with 3 independent, ensemble temperature reconstructions of the extra-tropical NH (Figures 6B, 6C). The 4 western US reconstructions show significant ($p<0.05$), positive agreement with the NH reconstructions over their common period of overlap (1730−1973). The strongest agreement occurs between the CR reconstruction and the multi-proxy summer (JJA) temperature reconstruction by Guillet et al. (2017) ($r =0.57$). We suspect that lower correlations between SR and the hemispheric reconstructions by Christiansen & Charpentier-Ljungqvist (2012) and Wilson et al. (2016) are partially due to differences in seasonality of input records, and potentially the decreased representation of low-latitude (<40°N) temperature-sensitive predictors in these NH estimates. Increasing the density of robust, local temperature records at lower latitudes of the NH may result in improved accuracy of future large-scale, ensemble NH temperature reconstructions in that they will be more representative of a greater latitudinal range for the NH. Both trends in asynchrony of regional temperature trends and differences between regional and large-scale models highlight the importance of regional temperature models for constraining the full range and variability of global temperature models.

4. Conclusions and future work

Using the LWB parameter, we provide 4 regional reconstructions of growing season T_{max} over much of the western North America temperate zone spanning the past *ca.* 300–400 years to present. Strong calibration/verification statistics for each reconstruction model indicates that LWB is a robust predictor of growing-season T_{max}, especially during late-summer. This LWB network provides paleo-temperature estimates which could further contribute increased understanding of the role of temperature on historical drought events, especially "hot droughts" (*e.g.* Overpeck 2013; Udall & Overpeck 2017) across the western US. As numerous temperature-sensitive MXD records exist across the western US, we suggest that future investigation of a multi-variate ensemble network of MXD, TRW, and LWB will considerably improve the current understanding of paleo-temperature across this portion of the NH network. While we have demonstrated the ability of LWB to contribute a collection of updated data points to the North American temperature proxy network, additional work is needed to extend the network back in time (*e.g.* sampling remnant or subfossil wood as in Luckman & Wilson 2005; Wiles et al. 2014; Gennaretti et al. 2014). Further, we posit that the continued exploration and application of BI methods at other mid-to-low latitude locations of the NH will contribute substantially to a more complete understanding of local to global climate histories and dynamics.

5. Acknowledgements

Dr. Christine Lucas, Jessie Mitchell, James McGee, and Dr. James Hardy Speer for field assistance at the RPS site; and April Kaiser and Ty Reinemann for field assistance at the FLS and MWS sites, Brian Van Winkle and the staff at the Dixie and Fishlake National Forests for assistance across multiple IP sites, Peter Brown, and the North American Dendroecological Fieldweek (NADEF) 2017–2020 instructors and participants for assistance with sample acquisition across the IP and CR regions, Joshua Bregy for assistance at the LOS and TLS sites. Reconstruction data are available at the National Centers for Environmental Information (NOAA).

References

Abatzoglou, J. T., & Williams, A. P. (2016). Impact of anthropogenic climate change on wildfire across western us forests. *Proceedings of the National Academy of Sciences*, *113*, 11770–11775.

Ahmed, M., Anchukaitis, K. J., Asrat, A., Borgaonkar, H. P., Braida, M., Buckley, B. M., Büntgen, U., Chase, B. M., Christie, D. A., Cook, E. R. et al. (2013). Continental-scale temperature variability during the past two millennia. *Nature geoscience*, *6*, 339–346.

Akaike, H. (1974). A new look at the statistical model identification. *IEEE transactions on automatic control*, *19*, 716–723.

Alday, J. G., Shestakova, T. A., de Dios, V. R., & Voltas, J. (2018). Dendrosync: An r package to unravel synchrony patterns in tree-ring networks. *Dendrochronologia*, *47*, 17–22.

Amburgey, S. M., Miller, D. A., Campbell Grant, E. H., Rittenhouse, T. A., Benard, M. F., Richardson, J. L., Urban, M. C., Hughson, W., Brand, A. B., Davis, C. J. et al. (2018). Range position and climate sensitivity: The structure of among-population demographic responses to climatic variation. *Global change biology*, *24*, 439–454.

Anchukaitis, K. J., D'Arrigo, R. D., Andreu-Hayles, L., Frank, D., Verstege, A., Curtis, A., Buckley, B. M., Jacoby, G. C., & Cook, E. R. (2013). Tree-ring-reconstructed summer temperatures from northwestern north america during the last nine centuries. *Journal of Climate*, *26*, 3001–3012.

Anchukaitis, K. J., Wilson, R., Briffa, K. R., Büntgen, U., Cook, E. R., D'Arrigo, R., Davi, N., Esper, J., Frank, D., Gunnarson, B. E. et al. (2017). Last millennium northern hemisphere summer temperatures from tree rings: Part ii, spatially resolved reconstructions. *Quaternary Science Reviews*, *163*, 1–22.

von Arx, G., Crivellaro, A., Prendin, A. L., Čufar, K., & Carrer, M. (2016). Quantitative wood anatomy—practical guidelines. *Frontiers in plant science*, *7*, 781.

Aukema, B. H., Werner, R. A., Haberkern, K. E., Illman, B. L., Clayton, M. K., & Raffa, K. F. (2005). Quantifying sources of variation in the frequency of fungi associated with spruce beetles: implications for hypothesis testing and sampling methodology in bark beetle–symbiont relationships. *Forest Ecology and Management*, *217*, 187–202.

Babst, F., Wright, W. E., Szejner, P., Wells, L., Belmecheri, S., & Monson, R. K. (2016). Blue intensity parameters derived from ponderosa pine tree rings characterize intra-annual density fluctuations and reveal seasonally divergent water limitations. *Trees*, *30*, 1403–1415.

Begum, S., Nakaba, S., Oribe, Y., Kubo, T., & Funada, R. (2010). Cambial sensitivity to rising temperatures by natural condition and artificial heating from late winter to early spring in the evergreen conifer cryptomeria japonica. *Trees*, *24*, 43–52.

Biondi, F., Perkins, D., Cayan, D., & Hughes, M. (1999). July temperature during the second millennium reconstructed from idaho tree rings. *Geophysical Research Letters*, *26*, 1445–1448.

Björklund, J., von Arx, G., Nievergelt, D., Wilson, R., Van den Bulcke, J., Günther, B., Loader, N., Rydval, M., Fonti, P., Scharnweber, T. et al. (2019). Scientific merits and analytical challenges of tree-ring densitometry. *Reviews of Geophysics*, .

Björklund, J., Gunnarson, B. E., Seftigen, K., Esper, J., & Linderholm, H. (2014). Blue intensity and density from northern fennoscandian tree rings, exploring the potential to improve summer temperature reconstructions with earlywood information. *Climate of the Past*, *10*, 877–885.

Björklund, J., Gunnarson, B. E., Seftigen, K., Zhang, P., & Linderholm, H. W. (2015). Using adjusted blue intensity data to attain high-quality summer temperature information: a case study from central scandinavia. *The Holocene*, *25*, 547–556.

Bond, G., Kromer, B., Beer, J., Muscheler, R., Evans, M. N., Showers, W., Hoffmann, S., Lotti-Bond, R., Hajdas, I., & Bonani, G. (2001). Persistent solar influence on north atlantic climate during the holocene. *science*, *294*, 2130–2136.

Briffa, K. R., Jones, P., & Schweingruber, F. (1992). Tree-ring density reconstructions of summer temperature patterns across western north america since 1600. *Journal of Climate*, *5*, 735–754.

Briffa, K. R., Jones, P. D., & Schweingruber, F. H. (1988). Summer temperature patterns over europe: a reconstruction from 1750 ad based on maximum latewood density indices of conifers. *Quaternary Research*, *30*, 36–52.

Briffa, K. R., Jones, P. D., Schweingruber, F. H., & Osborn, T. J. (1998). Influence of volcanic eruptions on northern hemisphere summer temperature over the past 600 years. *Nature*, *393*, 450–455.

Briffa, K. R., Osborn, T. J., & Schweingruber, F. (2004). Large-scale temperature inferences from tree rings: a review. *Global and planetary change*, *40*, 11–26.

Briffa, K. R., Osborn, T. J., Schweingruber, F. H., Harris, I. C., Jones, P. D., Shiyatov, S. G., & Vaganov, E. A. (2001). Low-frequency temperature variations from a northern tree ring density network. *Journal of Geophysical Research: Atmospheres*, *106*, 2929–2941.

Brönnimann, S., Franke, J., Nussbaumer, S. U., Zumbühl, H. J., Steiner, D., Trachsel, M., Hegerl, G. C., Schurer, A., Worni, M., Malik, A. et al. (2019). Last phase of the little ice age forced by volcanic eruptions. *Nature geoscience*, *12*, 650–656.

Buckley, B. M., Hansen, K. G., Griffin, K. L., Schmiege, S., Oelkers, R., D'Arrigo, R. D., Stahle, D. K., Davi, N., Nguyen, T. Q. T., Le, C. N. et al. (2018). Blue intensity from a tropical conifer's annual rings for climate reconstruction: An ecophysiological perspective. *Dendrochronologia*, *50*, 10–22.

Büntgen, U., Esper, J., Frank, D. C., Nicolussi, K., & Schmidhalter, M. (2005). A 1052-year tree-ring proxy for alpine summer temperatures. *Climate Dynamics*, *25*, 141–153.

Büntgen, U., Frank, D., Grudd, H., & Esper, J. (2008). Long-term summer temperature variations in the pyrenees. *Climate Dynamics*, *31*, 615–631.

Büntgen, U., Krusic, P. J., Verstege, A., Sangüesa-Barreda, G., Wagner, S., Camarero, J. J., Ljungqvist, F. C., Zorita, E., Oppenheimer, C., Konter, O. et al. (2017). New tree-ring evidence from the pyrenees reveals western mediterranean climate variability since medieval times. *Journal of Climate*, *30*, 5295–5318.

Cardoza, Y. J., Moser, J. C., Klepzig, K. D., & Raffa, K. F. (2008). Multipartite symbioses among fungi, mites, nematodes, and the spruce beetle, dendroctonus rufipennis. *Environmental Entomology*, *37*, 956–963.

Christiansen, B., & Charpentier-Ljungqvist, F. (2012). The extra-tropical northern hemisphere temperature in the last two millennia: reconstructions of low-frequency variability. *Climate of the Past*, *8*, 765–786.

Christiansen, B., & Ljungqvist, F. C. (2017). Challenges and perspectives for large-scale temperature reconstructions of the past two millennia. *Reviews of Geophysics*, *55*, 40–96.

Consortium, P. et al. (2017). A global multiproxy database for temperature reconstructions of the common era. *Scientific data*, *4*.

Cook, B. I., Miller, R. L., & Seager, R. (2008). Dust and sea surface temperature forcing of the 1930s "dust bowl" drought. *Geophysical Research Letters*, *35*.

Cook, E., & Briffa, K. (1990). A comparison of some tree-ring standardization methods.–cook, er, kairiukstis, la (eds.). methods of dendrochronology. applications in the environmental sciences.

Cook, E. R., & Holmes, R. (1996). Guide for computer program arstan. *The international tree-ring data bank program library version*, *2*, 75–87.

Cook, E. R., Krusic, P. J., Anchukaitis, K. J., Buckley, B. M., Nakatsuka, T., Sano, M. et al. (2013). Tree-ring reconstructed summer temperature anomalies for temperate east asia since 800 ce. *Climate Dynamics*, *41* , 2957–2972.

Cook, E. R., Meko, D. M., Stahle, D. W., & Cleaveland, M. K. (1999). Drought reconstructions for the continental united states. *Journal of Climate*, *12* , 1145–1162.

Cook, E. R., Seager, R., Cane, M. A., & Stahle, D. W. (2007). North american drought: Reconstructions, causes, and consequences. *Earth-Science Reviews*, *81*, 93–134.

Cook, E. R., Seager, R., Kushnir, Y., Briffa, K. R., Büntgen, U., Frank, D., Krusic, P. J., Tegel, W., van der Schrier, G., Andreu-Hayles, L. et al. (2015). Old world megadroughts and pluvials during the common era. *Science advances*, *1*, e1500561.

Cook, E. R., Solomina, O., Matskovsky, V., Cook, B. I., Agafonov, L., Berd-nikova, A., Dolgova, E., Karpukhin, A., Knysh, N., Kulakova, M. et al. (2020). The european russia drought atlas (1400–2016 ce). *Climate Dynamics*, *54* , 2317–2335.

Cook, E. R., Woodhouse, C. A., Eakin, C. M., Meko, D. M., & Stahle, D. W. (2004). Long-term aridity changes in the western united states. *Science*, *306* , 1015–1018.

Crowley, T. J., Zielinski, G., Vinther, B., Udisti, R., Kreutz, K., Cole-Dai, J., & Castellano, E. (2008). Volcanism and the little ice age. *PAGES news*, *16* , 22–23.

Cybis (2020). On blue channel measurements. https://www.cybis.se/forfun/dendro/helpcoorecorder7/bluechannel80/index.htm, accessed: 2020-03-30.

D'Arrigo, R., Jacoby, G., Frank, D., Pederson, N., Cook, E., Buckley, B., Nachin, B., Mijiddorj, R., & Dugarjav, C. (2001). 1738 years of mongolian temperature variability inferred from a tree-ring width chronology of siberian pine. *Geophysical Research Letters*, *28*, 543–546.

D'Arrigo, R., Wilson, R., & Anchukaitis, K. J. (2013). Volcanic cooling signal in tree ring temperature records for the past millennium. *Journal of Geophysical Research: Atmospheres*, *118*, 9000–9010.

D'Arrigo, R., Wilson, R., & Jacoby, G. (2006). On the long-term context for late twentieth century warming. *Journal of Geophysical Research: Atmospheres* , *111* .

D'Arrigo, R. D., & Jacoby, G. C. (1999). Northern north american tree-ring evidence for regional temperature changes after major volcanic events. *Climatic Change*, *41*, 1–15.

Davis, T. S., Horne, F. B., Yetter, J. C., & Stewart, J. E. (2018). Engelmann spruce chemotypes in colorado and their effects on symbiotic fungi associated

with the north american spruce beetle. *Journal of chemical ecology* , *44* , 601–610.

DeRose, R. J., Bentz, B. J., Long, J. N., & Shaw, J. D. (2013). Effect of increasing temperatures on the distribution of spruce beetle in engelmann spruce forests of the interior west, usa. *Forest Ecology and Management* , *308*, 198–206.

DeRose, R. J., Long, J. N., & Ramsey, R. D. (2011). Combining dendrochronological data and the disturbance index to assess engelmann spruce mortality caused by a spruce beetle outbreak in southern utah, usa. *Remote Sensing of Environment*, *115*, 2342–2349.

Deslauriers, A., Morin, H., & Begin, Y. (2003). Cellular phenology of annual ring formation of abies balsamea in the quebec boreal forest (canada). *Canadian Journal of Forest Research*, *33*, 190–200.

Dorado Liñán, I., Büntgen, U., González-Rouco, F., Zorita, E., Montávez, J., Gómez-Navarro, J., Brunet, M., Heinrich, I., Helle, G., & Gutiérrez, E. (2012). Estimating 750 years of temperature variations and uncertainties in the pyrenees by tree-ring reconstructions and climate simulations. *Climate of the Past*, *8*, 919–933.

Douglas, A. V., & Stockton, C. W. (1975). Long-term reconstruction of seasonal temperature and precipitation in the yellowstone national park region using dendroclimatic techniques, .

Eddy, J. A. (1976). The maunder minimum. *Science*, *192*, 1189–1202.

Edwards, J., Anchukaitis, K. J., Zambri, B., Andreu-Hayles, L., Oelkers, R., D'Arrigo, R., & von Arx, G. (2021). Intra-annual climate anomalies in northwestern north america following the 1783-1784 ce laki eruption. *Journal of Geophysical Research: Atmospheres*, (p. e2020JD033544).

Elliott, G. P. (2011). Influences of 20th-century warming at the upper tree line contingent on local-scale interactions: Evidence from a latitudinal gradient in the rocky mountains, usa. *Global Ecology and Biogeography*, *20*, 46–57.

Esper, J., Cook, E. R., & Schweingruber, F. H. (2002). Low-frequency signals in long tree-ring chronologies for reconstructing past temperature variability. *science*, *295*, 2250–2253.

Esper, J., Düthorn, E., Krusic, P. J., Timonen, M., & Büntgen, U. (2014). Northern european summer temperature variations over the common era from integrated tree-ring density records. *Journal of Quaternary Science, 29* , 487–494.

Esper, J., George, S. S., Anchukaitis, K., D'Arrigo, R., Ljungqvist, F. C., Luter-bacher, J., Schneider, L., Stoffel, M., Wilson, R., & Büntgen, U. (2018). Large-scale, millennial-length temperature reconstructions from tree-rings. *Dendrochronologia*, *50*, 81–90.

Esper, J., Klippel, L., Krusic, P. J., Konter, O., Raible, C. C., Xoplaki, E., Luterbacher, J., & Büntgen, U. (2020). Eastern mediterranean summer temperatures since 730 ce from mt. smolikas tree-ring densities. *Climate Dynamics, 54*, 1367–1382.

Fan, Z.-X., Bräuning, A., Yang, B., & Cao, K.-F. (2009). Tree ring density-based summer temperature reconstruction for the central hengduan mountains in southern china. *Global and Planetary Change, 65*, 1–11.

Flato, G., Marotzke, J., Abiodun, B., Braconnot, P., Chou, S., Collins, W., Cox, P., Driouech, F., Emori, S., Eyring, V. et al. (2013). Climate change 2013: the physical science basis. contribution of working group i to the fifth assessment report of the intergovernmental panel on climate change. *Evaluation of Climate Models, eds TF Stocker, D. Qin, G.-K. Plattner, M. Tignor, SK Allen, J. Boschung, et al.(Cambridge: Cambridge University Press)*, .

Frank, D., Esper, J., Zorita, E., & Wilson, R. (2010). A noodle, hockey stick, and spaghetti plate: a perspective on high-resolution paleoclimatology. *Wiley Interdisciplinary Reviews: Climate Change*, *1*, 507–516.

Fritts, H. (1976). *Tree rings and climate*. Elsevier.

Fuentes, M., Salo, R., Björklund, J., Seftigen, K., Zhang, P., Gunnarson, B., Aravena, J.-C., & Linderholm, H. W. (2018). A 970-year-long summer temperature reconstruction from rogen, west-central sweden, based on blue intensity from tree rings. *The Holocene*, *28*, 254–266.

Gärtner, H., & Nievergelt, D. (2010). The core-microtome: a new tool for surface preparation on cores and time series analysis of varying cell parameters. *Dendrochronologia*, *28*, 85–92.

Gennaretti, F., Arseneault, D., Nicault, A., Perreault, L., & Bégin, Y. (2014). Volcano-induced regime shifts in millennial tree-ring chronologies from northeastern north america. *Proceedings of the National Academy of Sciences*, *111*, 10077–10082.

George, S. S., & Ault, T. R. (2014). The imprint of climate within northern hemisphere trees. *Quaternary Science Reviews*, *89*, 1–4.

Gervais, B. R., & MacDonald, G. M. (2001). Tree-ring and summer-temperature response to volcanic aerosol forcing at the northern tree-line, kola peninsula, russia. *The Holocene*, *11*, 499–505.

González, J., & Valdés, J. B. (2003). Bivariate drought recurrence analysis using tree ring reconstructions. *Journal of Hydrologic Engineering*, *8*, 247–258.

Graumlich, L. J. (1993). A 1000-year record of temperature and precipitation in the sierra nevada. *Quaternary Research*, *39*, 249–255.

Graumlich, L. J., & Brubaker, L. B. (1986). Reconstruction of annual temperature (1590–1979) for longmire, washington, derived from tree rings. *Quaternary Research*, *25*, 223–234.

Griggs, R. F. (1914). Observations on the behavior of some species at the edges of their ranges. *Bulletin of the Torrey Botanical Club*, (pp. 25–49).

Gruber, A., Zimmermann, J., Wieser, G., & Oberhuber, W. (2009). Effects of climate variables on intra-annual stem radial increment in pinus cembra (l.) along the alpine treeline ecotone. *Annals of Forest Science*, *66*, 1–11.

Guillet, S., Corona, C., Stoffel, M., Khodri, M., Lavigne, F., Ortega, P., Eckert, N., Sielenou, P. D., Daux, V., Churakova, O. v. et al. (2017). Climate response to the samalas volcanic eruption in 1257 revealed by proxy records. *Nature geoscience*, *10*, 123–128.

Guttman, L. (1954). Some necessary conditions for common-factor analysis. *Psychometrika*, *19*, 149–161.

Harley, G. L., Grissino-Mayer, H. D., Franklin, J. A., Anderson, C., & Köse, N. (2012). Cambial activity of pinus elliottii var. densa reveals influence of seasonal insolation on growth dynamics in the florida keys. *Trees*, *26*, 1449–1459.

Harley, G. L., Heeter, K. J., Maxwell, J. T., Rayback, S. A., Maxwell, R. S., Reinemann, T. E., & H Taylor, A. (2020a). Towards broad-scale temperature reconstructions for eastern north america using blue light intensity from tree rings. *International Journal of Climatology*, .

Harley, G. L., Heeter, K. J., Maxwell, J. T., Rayback, S. A., Maxwell, R. S., Reinemann, T. E., & H Taylor, A. (2021). Towards broad-scale temperature reconstructions for eastern north america using blue light intensity from tree rings. *International Journal of Climatology*, *41*, E3142–E3159.

Harley, G. L., & Maxwell, J. T. (2018). Current declines of pecos river (new mexico, usa) streamflow in a 700-year context. *The Holocene*, *28*, 767–777.

Harley, G. L., Maxwell, R. S., Black, B. A., & Bekker, M. F. (2020b). A multi-century, tree-ring-derived perspective of the north cascades (usa) 2014–2016 snow drought. *Climatic Change*, (pp. 1–17).

Harris, I., Jones, P., Osborn, T., & Lister, D. (2014). Cru ts3. 22: Climatic research unit (cru) time-series (ts) version 3.22 of high resolution gridded data of month-by-month variation in climate (jan. 1901-dec. 2013). *NCAS British Atmospheric Data Centre, 24th September*, *2016*.

Heeter, K. J., Harley, G. L., Maxwell, J. T., McGee, J. H., & Matheus, T. J. (2020). Late summer temperature variability for the southern rocky mountains (usa) since 1735 ce: applying blue light intensity to low-latitude picea engelmannii parry ex engelm. *Climatic Change*, (pp. 1–24).

Heeter, K. J., Harley, G. L., Van De Gevel, S. L., & White, P. B. (2019). Blue intensity as a temperature proxy in the eastern united states: A pilot study from a southern disjunct population of picea rubens (sarg.). *Dendrochronologia*, *55*, 105–109.

Heeter, K. J., Rochner, M. L., & Harley, G. L. (2021). Summer air temperature for the greater yellowstone ecoregion (770–2019 ce) over 1,250 years. *Geophysical Research Letters*, *48*, e2020GL092269.

Hegerl, G., Luterbacher, J., González-Rouco, F., Tett, S. F., Crowley, T., & Xoplaki, E. (2011). Influence of human and natural forcing on european seasonal temperatures. *Nature Geoscience, 4*, 99–103.

Herrero, A., Rigling, A., & Zamora, R. (2013). Varying climate sensitivity at the dry distribution edge of pinus sylvestris and p. nigra. *Forest Ecology and Management*, *308*, 50–61.

Hill, J. K., Griffiths, H. M., & Thomas, C. D. (2011). Climate change and evolutionary adaptations at species' range margins. *Annual review of entomology*, *56*, 143–159.

Holmes, R. L. (1983). Computer-assisted quality control in tree-ring dating and measurement, .

Holt, R. D., & Keitt, T. H. (2005). Species' borders: a unifying theme in ecology. *Oikos, 108*, 3–6.

Husson, F., Josse, J., Le, S., Mazet, J., & Husson, M. F. (2016). Package 'factominer'. *An R package*, *96*, 698.

Jacoby, G. C., & D'Arrigo, R. (1989). Reconstructed northern hemisphere annual temperature since 1671 based on high-latitude tree-ring data from north america. *Climatic Change*, *14*, 39–59.

Jacoby, G. C., Workman, K. W., & D'Arrigo, R. D. (1999). Laki eruption of 1783, tree rings, and disaster for northwest alaska inuit. *Quaternary Science Reviews*, *18*, 1365–1371.

Jones, P., Briffa, K., Barnett, T., & Tett, S. (1998). High-resolution palaeoclimatic records for the last millennium: interpretation, integration and comparison with general circulation model control-run temperatures. *The Holocene*, *8*, 455–471.

Kaiser, H. F. (1960). The application of electronic computers to factor analysis. *Educational and psychological measurement*, *20*, 141–151.

Kalra, A., Piechota, T. C., Davies, R., & Tootle, G. A. (2008). Changes in us streamflow and western us snowpack. *Journal of Hydrologic Engineering*, *13*, 156–163.

Keyimu, M., Li, Z., Zhang, G., Fan, Z., Wang, X., & Fu, B. (2020a). Tree ring–based minimum temperature reconstruction in the central hengduan mountains, china. *Theoretical and Applied Climatology*, *141*, 359–370.

Keyimu, M., Li, Z., Zhao, Y., Dong, Y., Fu, B., Fan, Z., & Wang, X. (2020b). Reconstruction of maximum temperature on zhegu mountain, western sichuan plateau (china). *Climate Research*, *81*, 1–14.

Kipfmueller, K. F., & Salzer, M. W. (2010). Linear trend and climate response of five-needle pines in the western united states related to treeline proximity. *Canadian Journal of Forest Research*, *40*, 134–142.

Knudsen, M. F., Jacobsen, B. H., Seidenkrantz, M.-S., & Olsen, J. (2014). Evidence for external forcing of the atlantic multidecadal oscillation since termination of the little ice age. *Nature Communications*, *5*, 1–8.

Köse, N., Güner, H. T., Harley, G. L., & Guiot, J. (2017). Spring temperature variability over turkey since 1800 ce reconstructed from a broad network of tree-ring data. *Climate of the Past*, *13*, 1–15.

Kreutz, K. J., Mayewski, P. A., Meeker, L. D., Twickler, M. S., Whitlow, S. I., & Pittalwala, I. I. (1997). Bipolar changes in atmospheric circulation during the little ice age. *Science*, *277*, 1294–1296.

Larson, E. R., Allen, S., Flinner, N. L., Labarge, S. G., & Wilding, T. C. (2013). The need and means to update chronologies in a dynamic environment. *Tree-ring research*, *69*, 21–27.

Larsson, L. (2014). Coorecorder and cdendro programs of the coorecorder/cdendro package version 7.7. https://www.cybis.se/forfun/dendro.htm.

Lean, J., Skumanich, A., & White, O. (1992). Estimating the sun's radiative output during the maunder minimum. *Geophysical Research Letters* , *19* , 1591–1594.

Linderholm, H. W., Björklund, J., Seftigen, K., Gunnarson, B. E., & Fuentes, M. (2015). Fennoscandia revisited: a spatially improved tree-ring reconstruction of summer temperatures for the last 900 years. *Climate Dynamics*, *45* , 933–947.

Little, E. L., & Viereck, L. A. (1971). *Atlas of United States trees* volume 5. US Dept. of Agriculture, Forest Service.

Lloyd, A. H., & Fastie, C. L. (2002). Spatial and temporal variability in the growth and climate response of treeline trees in alaska. *Climatic Change*, *52* , 481–509.

Lücke, L. J., Hegerl, G. C., Schurer, A. P., & Wilson, R. (2019). Effects of memory biases on variability of temperature reconstructions. *Journal of Climate*, *32*, 8713–8731.

Luckman, B., & Wilson, R. (2005). Summer temperatures in the canadian rockies during the last millennium: a revised record. *Climate Dynamics*, *24*, 131–144.

Mann, M. E., Bradley, R. S., & Hughes, M. K. (1999). Northern hemisphere temperatures during the past millennium: Inferences, uncertainties, and limitations. *Geophysical research letters*, *26*, 759–762.

Mann, M. E., Zhang, Z., Rutherford, S., Bradley, R. S., Hughes, M. K., Shindell, D., Ammann, C., Faluvegi, G., & Ni, F. (2009). Global signatures and dynamical origins of the little ice age and medieval climate anomaly. *Science*, *326*, 1256–1260.

Martin, J. T., Pederson, G. T., Woodhouse, C. A., Cook, E. R., McCabe, G. J., Anchukaitis, K. J., Wise, E. K., Erger, P. J., Dolan, L., McGuire, M. et al. (2020). Increased drought severity tracks warming in the united states' largest river basin. *Proceedings of the National Academy of Sciences*, *117*, 11328–11336.

Masson-Delmotte, V., Schulz, M., Abe-Ouchi, A., Beer, J., Ganopolski, A., González Rouco, J., Jansen, E., Lambeck, K., Luterbacher, J., Naish, T. et al. (2013). Information from paleoclimate archives, .

Maxwell, J. T., Harley, G. L., Matheus, T. J., Strange, B. M., Van Aken, K., Au, T. F., & Bregy, J. C. (2020). Sampling density and date along with species selection influence spatial representation of tree-ring reconstructions. *Climate of the Past*, *16*, 1901–1916.

McCarroll, D., Pettigrew, E., Luckman, A., Guibal, F., & Edouard, J.-L. (2002). Blue reflectance provides a surrogate for latewood density of high-latitude pine tree rings. *Arctic, Antarctic, and Alpine Research*, *34*, 450–453.

McCullough, I. M., Davis, F. W., & Williams, A. P. (2017). A range of possibilities: Assessing geographic variation in climate sensitivity of ponderosa pine using tree rings. *Forest Ecology and Management*, *402*, 223–233.

Melvin, T. M., & Briffa, K. R. (2008). A "signal-free" approach to dendroclimatic standardisation. *Dendrochronologia*, *26*, 71–86.

Neukom, R., Gergis, J., Karoly, D. J., Wanner, H., Curran, M., Elbert, J., González-Rouco, F., Linsley, B. K., Moy, A. D., Mundo, I. et al. (2014). Inter-hemispheric temperature variability over the past millennium. *Nature Climate Change*, *4*, 362–367.

Neukom, R., Steiger, N., Gómez-Navarro, J. J., Wang, J., & Werner, J. P. (2019). No evidence for globally coherent warm and cold periods over the preindustrial common era. *Nature*, *571*, 550–554.

Oman, L., Robock, A., Stenchikov, G. L., Thordarson, T., Koch, D., Shindell, D. T., & Gao, C. (2006). Modeling the distribution of the volcanic aerosol cloud from the 1783–1784 laki eruption. *Journal of Geophysical Research: Atmospheres*, *111*.

Overpeck, J. T. (2013). The challenge of hot drought. *Nature*, *503*, 350–351.

Pederson, G. T., Gray, S. T., Woodhouse, C. A., Betancourt, J. L., Fagre, D. B., Littell, J. S., Watson, E., Luckman, B. H., & Graumlich, L. J. (2011). The unusual nature of recent snowpack declines in the north american cordillera. *science*, *333*, 332–335.

Pettit, J. M., Voelker, S. L., DeRose, R. J., & Burton, J. I. (2020). Spruce beetle outbreak was not driven by drought stress: Evidence from a tree-ring iso-demographic approach indicates temperatures were more important. *Global Change Biology*, *26*, 5829–5843.

Porter, T. J., Pisaric, M. F., Kokelj, S. V., & deMontigny, P. (2013). A ring-width-based reconstruction of june–july minimum temperatures since ad 1245

from white spruce stands in the mackenzie delta region, northwestern canada. *Quaternary Research*, *80*, 167–179.

Reid, E., & Wilson, R. (2020). Delta blue intensity vs. maximum density: A case study using pinus uncinata in the pyrenees. *Dendrochronologia*, (p. 125706).

Revelle, W. (1979). Hierarchical cluster analysis and the internal structure of tests. *Multivariate Behavioral Research*, *14*, 57–74.

Rydval, M., Druckenbrod, D. L., Svoboda, M., Trotsiuk, V., Janda, P., Mikoláš, M., Čada, V., Bače, R., Teodosiu, M., & Wilson, R. (2018). Influence of sampling and disturbance history on climatic sensitivity of temperature-limited conifers. *The Holocene*, *28*, 1574–1587.

Rydval, M., Larsson, L.-Å., McGlynn, L., Gunnarson, B. E., Loader, N. J., Young, G. H., & Wilson, R. (2014). Blue intensity for dendroclimatology: should we have the blues? experiments from scotland. *Dendrochronologia*, *32*, 191–204.

Rydval, M., Loader, N. J., Gunnarson, B. E., Druckenbrod, D. L., Linderholm, H. W., Moreton, S. G., Wood, C. V., & Wilson, R. (2017). Reconstructing 800 years of summer temperatures in scotland from tree rings. *Climate Dynamics*, *49*, 2951–2974.

Salzer, M. W., Bunn, A. G., Graham, N. E., & Hughes, M. K. (2014a). Five millennia of paleotemperature from tree-rings in the great basin, usa. *Climate Dynamics*, *42*, 1517–1526.

Salzer, M. W., Larson, E. R., Bunn, A. G., & Hughes, M. K. (2014b). Changing climate response in near-treeline bristlecone pine with elevation and aspect. *Environmental Research Letters*, *9*, 114007.

Schmidt, A., Thordarson, T., Oman, L. D., Robock, A., & Self, S. (2012). Climatic impact of the long-lasting 1783 laki eruption: Inapplicability of mass-independent sulfur isotopic composition measurements. *Journal of Geophysical Research: Atmospheres*, *117*.

Schneider, L., Smerdon, J. E., Büntgen, U., Wilson, R. J., Myglan, V. S., Kirdyanov, A. V., & Esper, J. (2015). Revising midlatitude summer temperatures back to ad 600 based on a wood density network. *Geophysical Research Letters, 42*, 4556–4562.

Schurer, A. P., Hegerl, G. C., Luterbacher, J., Brönnimann, S., Cowan, T., Tett, S. F., Zanchettin, D., & Timmreck, C. (2019). Disentangling the causes of the 1816 european year without a summer. *Environmental Research Letters , 14*, 094019.

Schweingruber, F., Briffa, K., & Nogler, P. (1993). A tree-ring densitometric transect from alaska to labrador. *International Journal of Biometeorology, 37*, 151–169.

Schweingruber, F., Fritts, H., Bräker, O., Drew, L., & Schär, E. (1978). The x-ray technique as applied to dendroclimatology, .

Schweingruber, F. H., & Briffa, K. R. (1996). Tree-ring density networks for climate reconstruction. In *Climatic variations and forcing mechanisms of the last 2000 years* (pp. 43–66). Springer.

Shindell, D. T., Schmidt, G. A., Mann, M. E., Rind, D., & Waple, A. (2001). Solar forcing of regional climate change during the maunder minimum. *science, 294*, 2149–2152.

Six, D. L., & Bentz, B. J. (2003). Fungi associated with the north american spruce beetle, dendroctonus rufipennis. *Canadian Journal of Forest Research, 33*, 1815–1820.

Stoffel, M., Khodri, M., Corona, C., Guillet, S., Poulain, V., Bekki, S., Guiot, J., Luckman, B. H., Oppenheimer, C., Lebas, N. et al. (2015). Estimates of volcanic-induced cooling in the northern hemisphere over the past 1,500 years. *Nature Geoscience, 8*, 784.

Stott, P. A., Gillett, N. P., Hegerl, G. C., Karoly, D. J., Stone, D. A., Zhang, X., & Zwiers, F. (2010). Detection and attribution of climate change: a regional perspective. *Wiley Interdisciplinary Reviews: Climate Change*, *1*, 192–211.

Thuiller, W. (2004). Patterns and uncertainties of species' range shifts under climate change. *Global Change Biology*, *10*, 2020–2027.

Tingley, M. P., Craigmile, P. F., Haran, M., Li, B., Mannshardt, E., & Rajaratnam, B. (2012). Piecing together the past: Statistical insights into paleoclimatic reconstructions. *Quaternary Science Reviews*, *35*, 1–22.

Trotsiuk, V., Pederson, N., Druckenbrod, D. L., Orwig, D. A., Bishop, D. A., Barker-Plotkin, A., Fraver, S., & Martin-Benito, D. (2018). Testing the efficacy of tree-ring methods for detecting past disturbances. *Forest Ecology and Management*, *425*, 59–67.

Trouet, V., & Van Oldenborgh, G. J. (2013). Knmi climate explorer: a web-based research tool for high-resolution paleoclimatology. *Tree-Ring Research*, *69*, 3–14.

Udall, B., & Overpeck, J. (2017). The twenty-first century colorado river hot drought and implications for the future. *Water Resources Research*, *53*, 2404–2418.

US Climate Data (2020). Climate ruidoso- new mexico. Data retrieved from https://www.usclimatedata.com/climate/ruidoso/new-mexico/united-states/usnm0270.

Vinod, H. D., López-de Lacalle, J. et al. (2009). Maximum entropy bootstrap for time series: the meboot r package. *Journal of Statistical Software*, *29*, 1–19.

Wagner, S., & Zorita, E. (2005). The influence of volcanic, solar and co 2 forcing on the temperatures in the dalton minimum (1790–1830): a model study. *Climate Dynamics*, *25*, 205–218.

Wahl, E. R., & Ammann, C. M. (2007). Robustness of the mann, bradley, hughes reconstruction of northern hemisphere surface temperatures: Examination of criticisms based on the nature and processing of proxy climate evidence. *Climatic change*, *85*, 33–69.

Wild, M. (2009). Global dimming and brightening: A review. *Journal of Geophysical Research: Atmospheres*, *114*.

Wiles, G., Charlton, J., Wilson, R. J., DArrigo, R., Buma, B., Krapek, J., Gaglioti, B. V., Wiesenberg, N., & Oelkers, R. (2019). Yellow-cedar blue intensity tree ring chronologies as records of climate, juneau, alaska, usa. *Canadian Journal of Forest Research*, .

Wiles, G. C., D'Arrigo, R. D., Barclay, D., Wilson, R. S., Jarvis, S. K., Vargo, L., & Frank, D. (2014). Surface air temperature variability reconstructed with tree rings for the gulf of alaska over the past 1200 years. *The Holocene*, *24* , 198–208.

Williams, A. P., Cook, E. R., Smerdon, J. E., Cook, B. I., Abatzoglou, J. T., Bolles, K., Baek, S. H., Badger, A. M., & Livneh, B. (2020). Large contribution from anthropogenic warming to an emerging north american megadrought. *Science*, *368*, 314–318.

Wilson, R., Anchukaitis, K., Andreu-Hayles, L., Cook, E., D'Arrigo, R., Davi, N., Haberbauer, L., Krusic, P., Luckman, B., Morimoto, D. et al. (2019). Improved dendroclimatic calibration using blue intensity in the southern yukon. *The Holocene*, (p. 0959683619862037).

Wilson, R., Anchukaitis, K., Briffa, K. R., Büntgen, U., Cook, E., D'arrigo, R., Davi, N., Esper, J., Frank, D., Gunnarson, B. et al. (2016). Last millennium northern hemisphere summer temperatures from tree rings: Part i: The long term context. *Quaternary Science Reviews*, *134*, 1–18.

Wilson, R., D'Arrigo, R., Andreu-Hayles, L., Oelkers, R., Wiles, G., Anchukaitis, K., & Davi, N. (2017). Experiments based on blue intensity for

reconstructing north pacific temperatures along the gulf of alaska. *Climate of the Past*, .

Wilson, R., Rao, R., Rydval, M., Wood, C., Larsson, L.-Å., & Luckman, B. H. (2014). Blue intensity for dendroclimatology: The bc blues: A case study from british columbia, canada. *The Holocene*, *24*, 1428–1438.

Wilson, R. J., & Luckman, B. H. (2003). Dendroclimatic reconstruction of maximum summer temperatures from upper treeline sites in interior british columbia, canada. *The Holocene*, *13*, 851–861.

Woodhouse, C. A., Meko, D. M., MacDonald, G. M., Stahle, D. W., & Cook, E. R. (2010). A 1,200-year perspective of 21st century drought in southwestern north america. *Proceedings of the National Academy of Sciences* , *107* , 21283–21288.

Zambri, B., Robock, A., Mills, M. J., & Schmidt, A. (2019). Modeling the 1783–1784 laki eruption in iceland: 1. aerosol evolution and global stratospheric circulation impacts. *Journal of Geophysical Research: Atmospheres* , *124* , 6750–6769.

Zhai, P., Zhou, B., & Chen, Y. (2018). A review of climate change attribution studies. *Journal of Meteorological Research*, *32*, 671–692.

1 Tables and Figures

Table 1: **Information for sample sites (*n* =26) examined for the western US latewood blue intensity network.** State Codes: Idaho: ID, Montana: MT, Wyoming: WY, Utah: UT, Colorado: CO, and New Mexico: NM.*Site numbers correspond to labels in Figure 1. Replication (Rep) indicates number of trees for each LWB chronology required to attain EPS >0.85, Years represents the timespan of each chronology using the EPS >0.85 threshold. We also include the average RBAR of each chronology and the optimum Pearson's correlations (*p*<0.05) for 1920-present (1970-present) for each LWB chronology against the local 0.5°(or larger where relevant) CRU TS 4.04 (Harris et al. 2014) maximum temperature grid.

Site #	Site code	US State	Lat. (°N)	Lon. (°E)	Elev. (m)	Rep	Years	RBAR	Corr. Tmax (post 1970)
1	BFL	ID	48.88	-116.81	2282	3	1721-2019	0.54	Aug: 0.61 (0.68)
2	MCO	ID	46.80	-116.86	2963	5	1920-2019	0.34	JAS: 0.43 (0.37)
3	FKY	MT	45.50	-111.67	1930	10	1901-2000	0.26	Mar-Aug: 0.56 (0.61)
4	FLS	WY	44.91	-109.53	2959	7	1766-2016	0.28	JJA: 0.64 (0.68)
5	RPS	WY	44.99	-109.92	3046	8	1781-2017	0.27	JJA: 0.67 (0.67)
6	MWS	WY	44.80	-110.43	2960	8	1760-2019	0.29	JJA: 0.52 (0.59)
7	BTP	WY	44.57	-109.29	3010	5	1756-2015	0.39	JJA: 0.65 (0.61)
8	CBS	WY	44.57	-109.37	2945	6	1730-2015	0.34	JJAS: 0.65 (0.61)
9	TOW	WY	44.54	-109.31	2960	7	1850-2015	0.28	Aug: 0.64 (0.70)
10	MBP	WY	41.21	-109.29	3225	9	1909-2015	0.26	Aug: 0.53 (0.55)
11	MON	UT	38.60	-111.96	3122	6	1886-2016	0.32	Apr-Aug: 0.60 (0.61)
12	TUS	UT	38.36	-112.38	3263	3	1667-2011	0.49	Apr-Aug: 0.53 (0.50)
13	TLM	UT	38.41	-111.47	3436	8	1848-2016	0.27	Apr-Aug: 0.51 (0.57)
14	BUP	UT	37.32	-113.50	3438	3	1654-2018	0.65	AM: 0.47 (0.52)
15	PLS	UT	38.07	-111.56	3280	13	1891-2000	0.26	AM: 0.47 (0.47)
16	HAY	UT	38.49	-109.25	3271	6	1861-2017	0.32	Apr-Aug: 0.49 (0.59)
17	ABA	UT	37.84	-109.46	3425	4	1859-2002	0.42	Apr-Aug: 0.45 (0.50)
18	MDB	CO	40.21	-105.29	3300	4	1659-2015	0.43	AS: 0.46 (0.53)
19	CPI	CO	38.82	-106.40	3580	4	1778-2015	0.43	Jun-Sep: 0.54 (0.62)
20	PPL	CO	38.52	-105.42	3460	7	1732-2015	0.30	Aug: 0.36 (0.53)
21	PPU	CO	38.52	-105.42	3550	3	1623-2015	0.53	Aug: 0.54 (0.61)
22	WHE	NM	36.55	-105.41	3708	5	1803-2015	0.39	AS: 0.57 (0.59)
23	JIS	NM	36.18	-105.56	3587	6	1776-2014	0.32	AS: 0.56 (0.62)
24	SLE	NM	36.04	-105.54	3594	7	1848-2014	0.28	Aug: 0.39 (0.43)
25	TLS	NM	35.99	-105.64	3573	5	1694-2018	0.36	Aug: 0.53 (0.58)
26	LOS	NM	33.39	-105.81	3760	4	1878-2018	0.35	AS: 0.65 (0.73)

Table 2: **Summary statistics for PC regressions of each region included in the western US latewood blue intensity network.** (Top) Calibration and verification periods, monthly duration of the reconstructed season, and the final reconstructed period for each regional model. (Bottom) measures of explained variance for each regional model: RSQ (calibration period coefficient of multiple determination), VRE (validation period reduction of error), VCE (validation period coefficient of efficiency) and RMSE (root mean squared error).

	Calibration period	Verification Period	Target months	Reconstructed Period	#forward nests	#backward nests
NR	1966-2000	1920-1965	MJJA	1721-2018	1	2
CR	1966-2015	1920-1965	MJJAS	1730-2018	3	4
IP	1966-2000	1920-1965	AMJJAS	1654-2018	4	7
SR	1966-2014	1920-1965	AS	1623-2018	2	7

	Model	First Year	Last Year	RSQ	VRE	VCE	RMSE
	NR	1920	2000	0.53	0.55	0.53	0.80
	CR	1850	2015	0.44	0.44	0.44	0.84
	IP	1909	2000	0.49	0.55	0.54	0.62
	SR	1878	2014	0.54	0.53	0.52	0.65

Table 3: **Results of severity-duration analysis showing the top-five ranking warmest (+, top row) and coolest (-, bottom row) single-year anomalies (left) and event periods (right) for the each region.** Single-year anomalies calculated over the full period (NR: 1730-2018, CR: 1680-2018, IP: 1646-2018, and SR: 1622-2018). Duration indicates the number of years of each event, as calculated by the severity-duration analysis from reconstructed values. Magnitude = mean cumulative departure from the long-term reconstructed mean for each region; Intensity = duration (years) divided by the magnitude; after ranking, overall score = duration rank + intensity rank. Periods of interest are color coded: red= recent warming trend; orange= Dust Bowl; blue= Maunder Minimum; purple= Dalton Minimum.

Rank	Year	1-year Anomaly	Period	Duration (years)	Magnitude	Intensity	Duration Rank	Magnitude Rank	Overall Score
				Northern Rocky Mountains					
1	1979,1910	+1.70	1773-1786	14	+6.73	+0.48	9	68	77
2	1940	+1.65	1930-1936	7	+6.80	+0.97	6	69	75
3	1936	+1.63	1888-1898	11	+5.68	+0.52	8	66	74
4	1931	+1.49	1908-1915	8	+6.20	+0.77	7	67	74
5	1958	1.47	1938-1942	5	+5.62	+1.12	5	65	70
1	1964	-4.63	1879-1884	6	-5.45	-0.91	6	69	75
2	1899	-3.65	1818-1826	9	-4.90	-0.54	7	67	74
			1810-1815	6	-4.32	-0.72	6	65	71
3	1907	-2.96							
4	1954	-2.57	1974-1976	3	-5.06	-1.69	3	68	71
5	1876	-2.52	1964-1965	2	-4.82	-2.41	2	66	68
				Central Rocky Mountains					
1	2016	+3.08	1928-1940	13	+13.74	+1.06	9	69	78
2	2017	+2.18	1888-1898	11	+6.38	+0.58	8	67	75
3	1949	+2.08	2015-2018	4	+7.50	+1.87	4	68	72
4	1988	+1.99	1869-1874	6	+4.31	+0.72	6	65	71
5	1748	+1.81	1946-1950	5	+5.31	+1.06	5	66	71
1	1968	-4.52	1834-1849	16	-17.71	-1.11	7	68	75
2	1993	-3.16	1972-1980	9	-8.27	-0.92	6	67	73
3	1787	-2.77	1904-1908	5	-5.44	-1.09	5	66	71
4	1838	-2.74	1915-1918	4	-4.03	-1.01	4	64	68
5	1951	-2.57	1967-1968	2	-4.54	-2.27	2	65	67
				Intermontane Plateaus					
1	1669	+3.08	1767-1777	11	+7.97	+0.72	9	94	103
2	1690	+2.32	1664-1669	6	+8.08	+1.35	6	95	101
3	2017	+2.28	1931-1940	10	+5.14	+0.51	8	92	100
4	1729	+2.12	1711-1719	9	+4.65	0.52	7	91	98
5	1783	+2.06	2015-2018	4	+6.28	+1.57	4	93	97
1	1965	-3.83	1818-1824	7	-6.56	-0.94	7	94	101
2	1746	-2.41	1654-1659	6	-9.20	-1.53	6	95	101
3	1657	-2.23	1676-1678	3	-4.75	-1.58	3	93	96
4	1763	-2.17	1758-1761	4	-3.87	-0.97	4	91	95
5	1736	-2.13	1963-1965	3	-4.75	-1.58	3	92	95
				Southern Rocky Mountains					
1	2018	+3.52	1894-1905	12	+12.77	+1.06	9	73	82
2	1632, 1902	+2.27	1942-1954	13	+7.33	+0.56	10	71	81
3	1900	+2.00	1859-1865	7	+6.31	+0.90	7	70	77
4	1856	+1.92	2015-2018	4	+7.48	+1.87	4	72	76
5	2017	+1.72	1715-1722	8	+5.57	+0.70	8	68	76
1	1646	-4.33	1641-1656	16	-20.50	-1.28	10	73	83
2	1761	-3.39	1970-1984	15	-12.33	-0.82	9	72	81
3	1831	-3.33	1805-1813	9	-9.07	-1.01	8	70	78
4	1647	-2.81	1963-1968	6	-9.20	-1.53	5	71	76
5	1645	-2.66	1758-1764	7	-8.87	-1.27	6	69	75
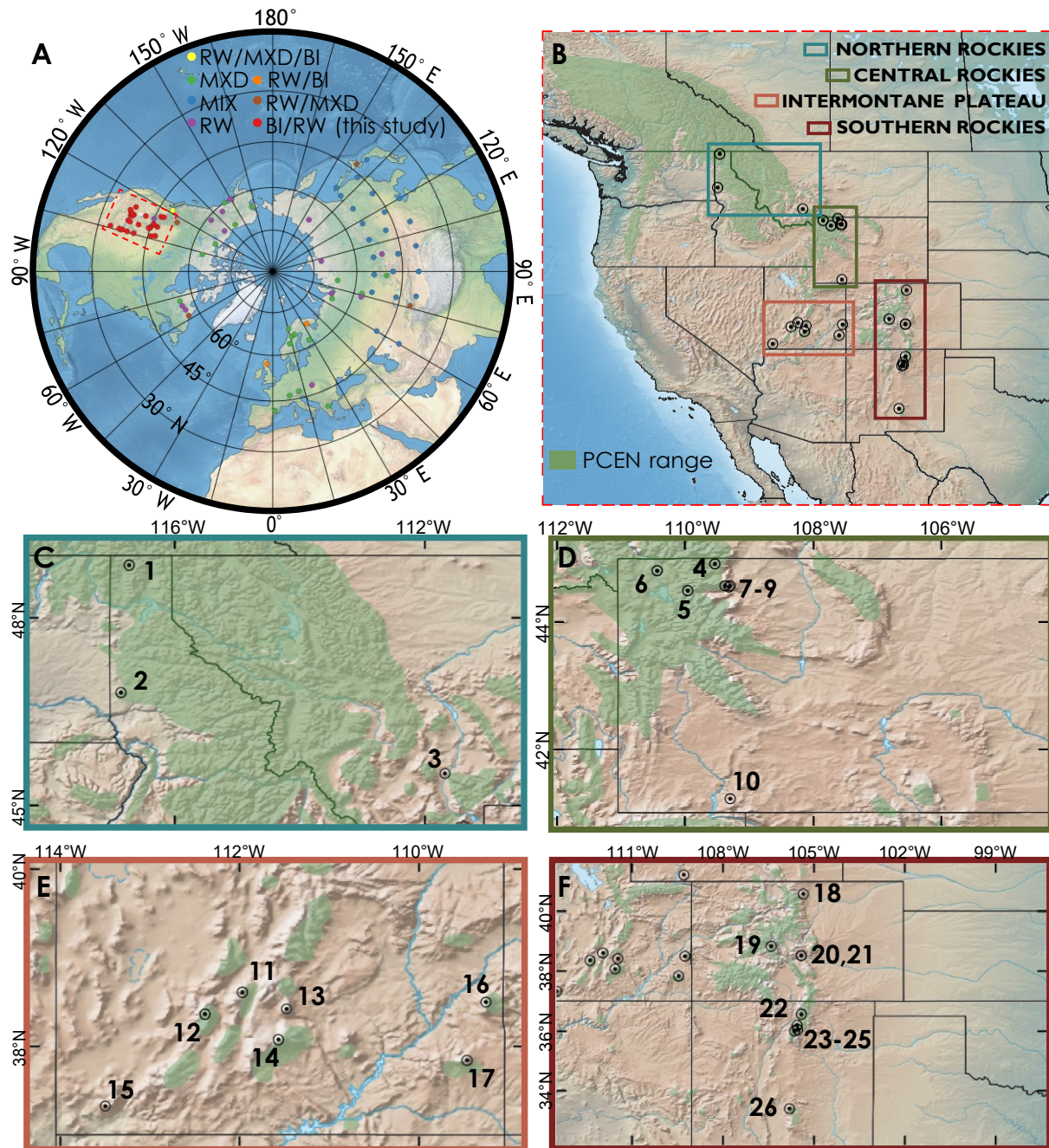
Figure 1: **Global-spatial context of the western US blue intensity network.** A) Location and data-classification of temperature-sensitive, tree-ring datasets currently included in the recent N-TREND network compiled by Wilson et al. (2016), as well as the 26 LWB chronology sites presented in this study (red circles). Map insets (B-F) displaying the locations of all 26 sites examined in this study sorted by physiographic region, as well as the species range of *Picea engelmannii* (green polygon) as indicated by Little and Viereck (1971). Chronologies are clustered by hierarchical cluster analysis into 4 regions (Figure S2): US Northern Rocky Mountains (teal), Central Rocky Mountains (green), Intermontane Plateau (salmon), and Southern Rocky Mountains (dark red). Numbers correspond to respective chronology information and statistics displayed in Table 1.
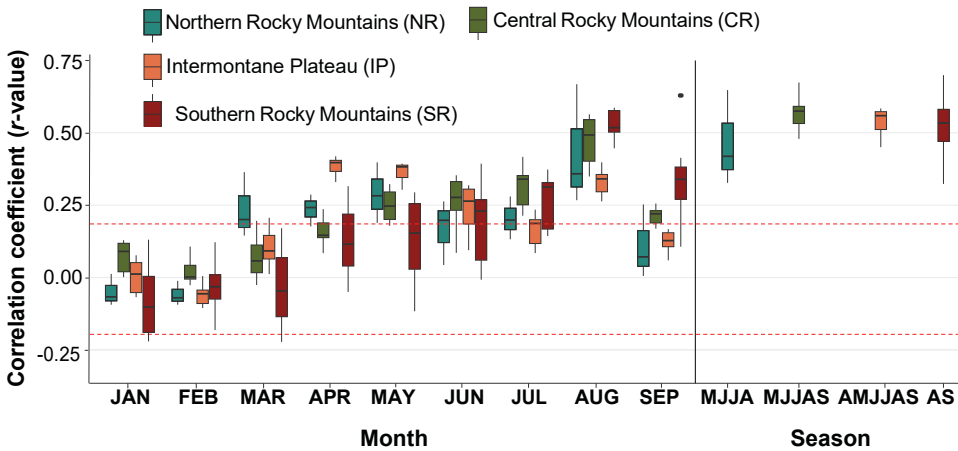
Figure 2: **Correlations (Pearson's *r*) between maximum temperature and (T_max) late-wood blue intensity (LWB) chronologies across the western US network, grouped by region.** Pearson's *r* between all LWB chronologies across each region and current-year monthly regional target CRU 4.04 0.5°T_max data (Harris et al., 2014) for each region (NR: 45.0-49.0°N, 117.0-111.5°W; CR: 44.0-45.0°N, 111.0-109.0°W; IP: 37.0-41.5°N, 114.0-109.0°W; SR: 33.0-40.5°N, 106.0-105.0°W), and the optimum seasonal average of regional target CRU 4.04 0.5°T_max data. Correlations span the common period between the starting calibration year (1920) and the last year of each individual chronology. Dashed red lines indicate significance at the *p*<0.05 level.
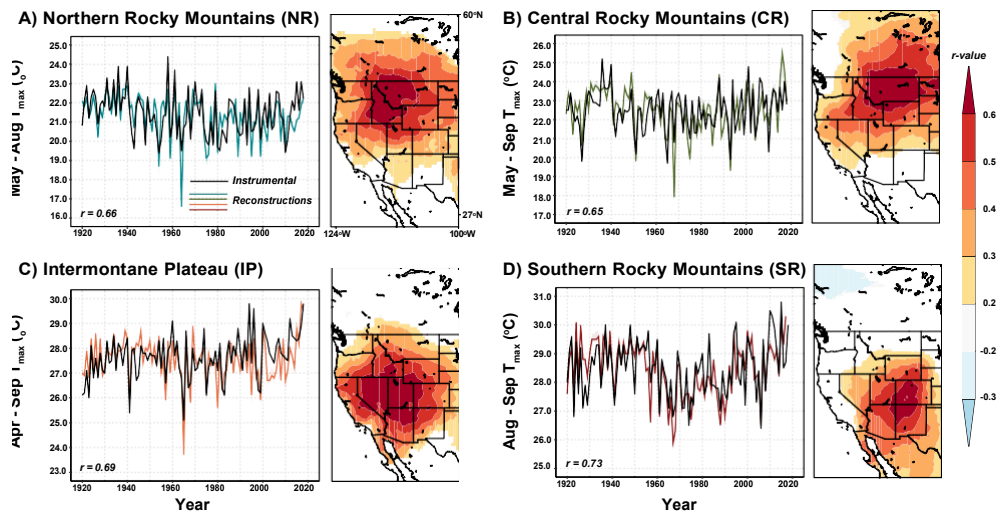

Figure 3: **Temporal and spatial relationships between 4 western US regional maximum temperature (T_max) reconstructions and instrumental data.** The temporal relationship (Pearson's *r*, *p*<0.05) between the regional reconstructions (colored lines, line shading represents standard error) and the CRU TS 4.04 T_max data (black line) (Harris et al., 2014) over the period spanning 1920-2018. We also include the extent of the spatial distribution of correlations between the predictor and predictand temperature data for each regional model over the period 1920-2018 (Pearson's r, significant at *p*<0.05 level).
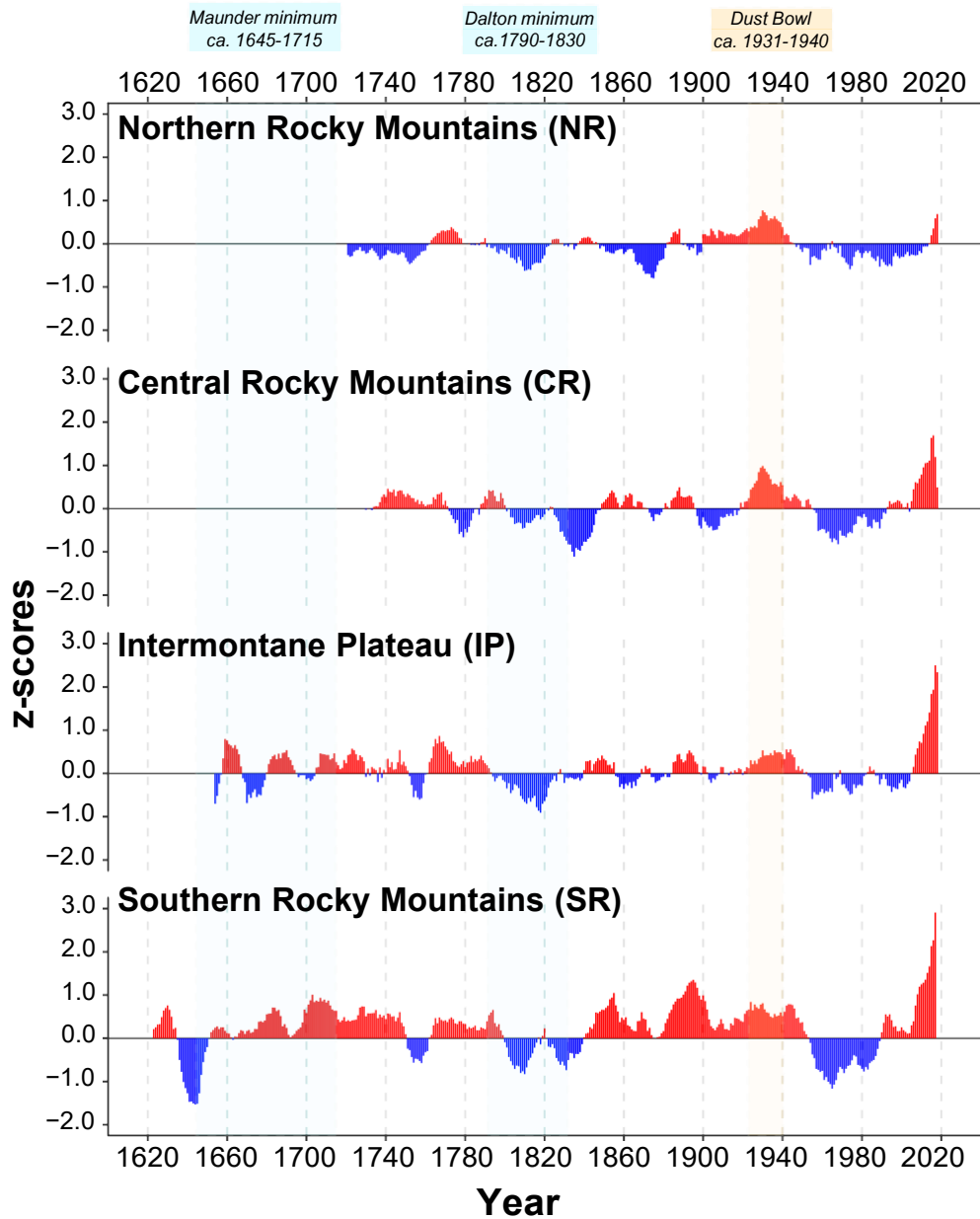
5

Figure 4: **Decadal-scale variability of 4 regional temperature reconstructions derived from the western US latewood blue intensity network.** Temperature anomalies calculated as z-scores from the mean and standard deviation of the common period of all reconstructions (1730−2018) for each region. Notable cool and warm periods (Maunder and Dalton Minima and the Dust Bowl) are highlighted. Z-scores are smoothed with an 11-year running average. Warm years are indicated by red and cool years are indicated by blue.
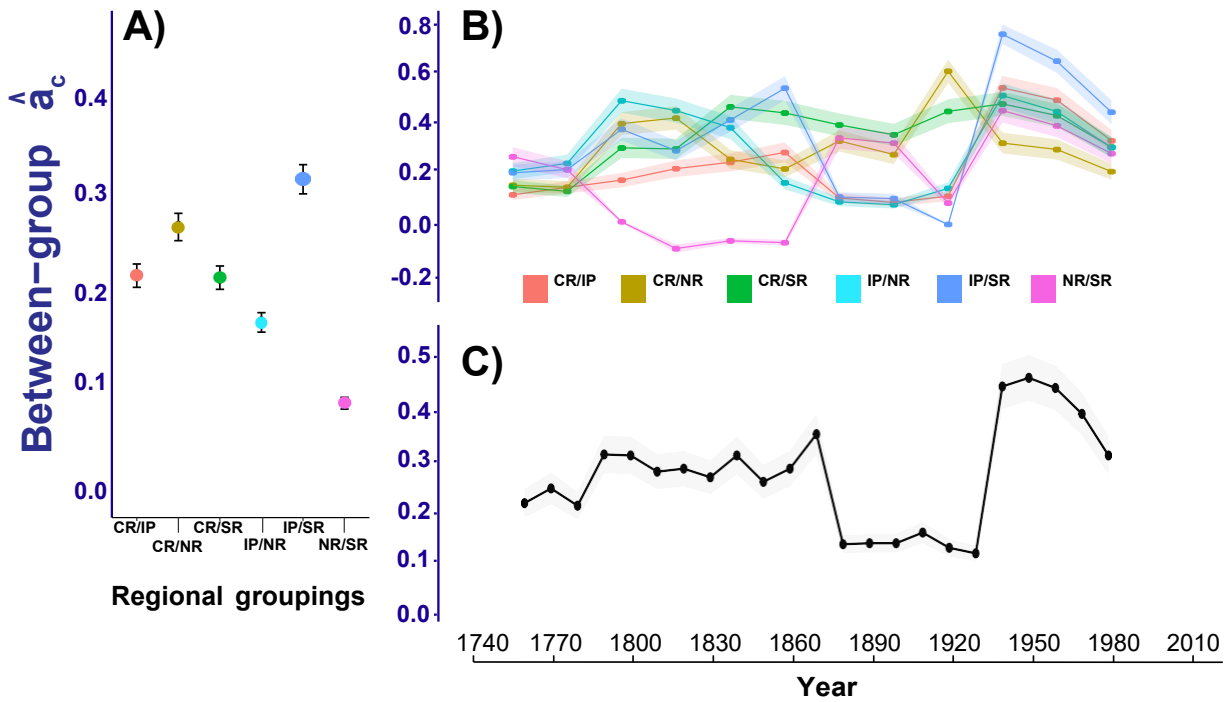
Figure 5: **Comparison and evaluation of synchrony between 4 regional temperature reconstructions.** We compare between-group synchrony (the estimated proportion of common inter-annual variance; $\hat{a}_c$) of A) individual pairings of the 4 regional reconstructions (raw reconstructed values) averaged over the entire common reconstructed period (1730-2018), B) time series of between-group synchrony trends between all 4 regional reconstructions using a 60-year window and 10-year lag (based on AIC criteria), and C) time series of between group synchrony trends of regional reconstruction pairings listed from B) using a 60-year window and 10-year lag (based on AIC criteria) over the common period (1730-2018). The error bars in A) and shadows in B) and C) depict the standard errors.
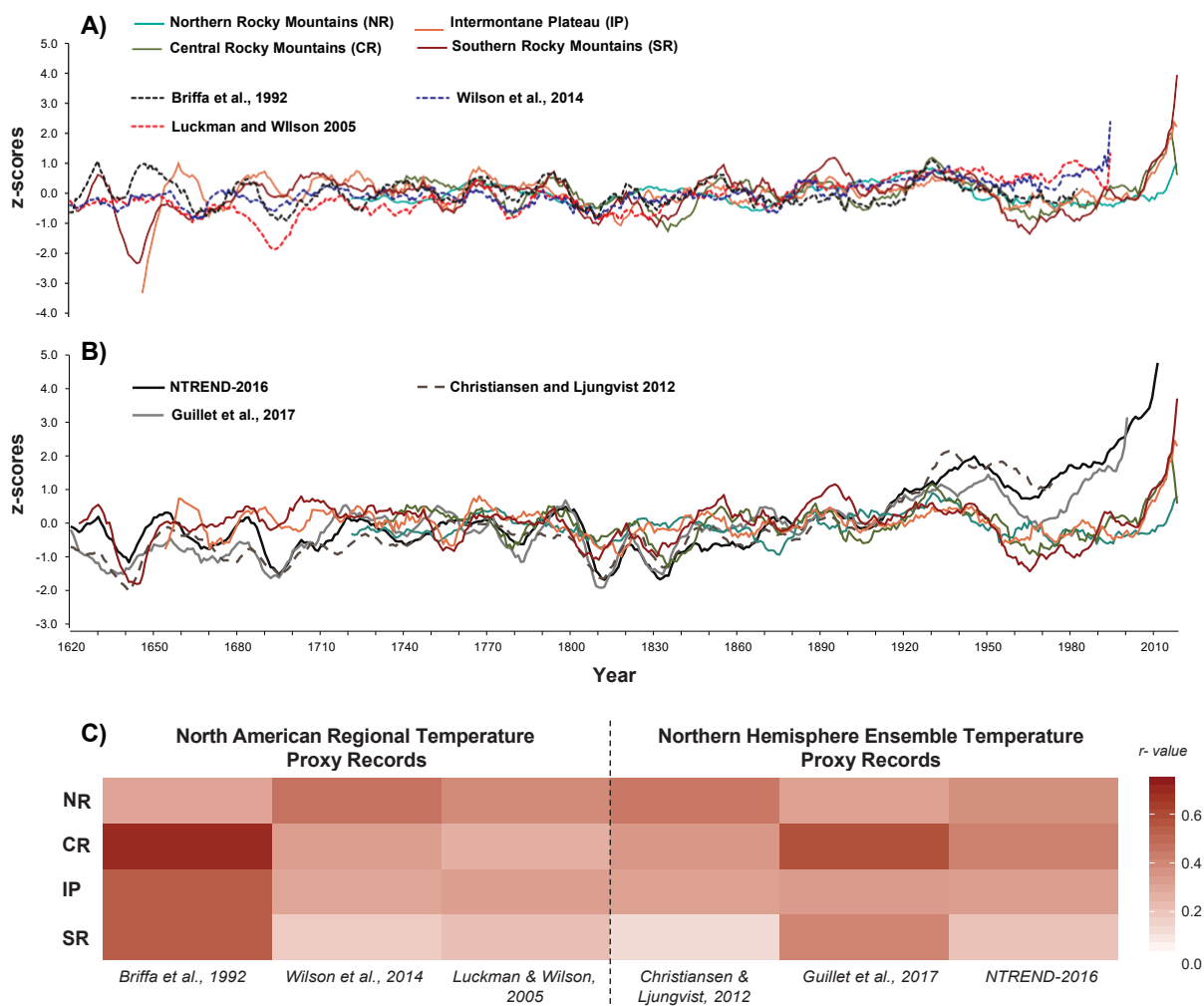
Figure 6: **Coherence of 4 western US temperature reconstructions with independent regional- and large-scale paleo-temperature reconstructions.** Comparison of plotted time series (as z-scores) between the 4 western US regional temperature reconstructions with A) 3 independent regional temperature reconstructions from North America: Western US (Briffa et al., 1992), Alberta, Canada (Luckman and Wilson 2005), and British Columbia, Canada (Wilson et al., 2014), and with B) 3 independent ensemble temperature reconstructions for the Northern Hemisphere: N-TREND 2016 (Wilson et al., 2016), Guillet et al., 2017, and Christiansen and Ljungvist 2012. All time series displayed as z-scores calculated over the common period for all records (1730-1973) and smoothed with an 11-year running average. C) Correlation matrix (Pearsons r-value) over the common period 1730-1973 between the 4 regional reconstructions from this study and the independent records listed in A) and B). All values in the matrix are significant at the $p < 0.05$ level.